Petrography and Geochemistry of Cherts, Al Jabal al Akhdar, NE Libya.

By

Mailod Ahmed Mohammed Baker

Supervisor

Dr. Osama R. Shaltami

Dr. Ahmed M. Muftah

This Thesis was submitted in Partial Fulfillment of the Requirements for

Master's Degree of Science in Geology.

University of Benghazi

Faculty of Science

September 2017

الخصائص الصخرية والكيميائية لصخور الصوان شمال شرق ليبيا

إعــداد/ ميلود احمد محمد بكار

لجنة الاشراف والمناقشة:

د. اسامة رحيل الشلطامي	مشرفا
د. أحمد مفتاح الكوافي	مشرفا مساعد
د. نبيل رمضان بدر	ممتحنا داخليا
د. حمد عمر الورفلي	ممتحنا خارجيا

قدمت هذه الرسالة استكمالا لمتطلبات درجة الماجستير في الجيولوجيا بكلية العلوم/جامعة بنغازي بتاريخ 17 سبتمبر 2017 م.

Dedication

For my mother

Ministry of Education

University of Benghazi

Directorate of Graduate Studies

Faculty of Science

Department of Earth sciences

This Thesis (**Petrography and Geochemistry of Cherts, Al Jabal al Akhdar, NE Libya**.) was Successfully Defended and Approved on 17-9-2017.

Examination Committee	**Signature**
Dr. Osama R. Shaltami, (Supervisor)	……..
Dr. Ahmed M. Muftah, (co-Supervisor)	……..……
Dr. Nabil R. Bader, (internal examiner)	……...
Dr. Hamad O. Elwerfali, (external examiner)	……..……..…….....

Director of Graduate studies & Training

ACKNOWLEDGEMENT

Before anything and foremost, I would like to thank Allah for everything and anything, also for giving us an opportunity taking this path of earth science.

Firstly, I am deeply indebted to my supervisors Dr. Ahmed Muftah Associated Professor of Paleontology and Dr. Osama El Sheltami Associated Professor of geochemistry in Department of the Earth Sciences, Benghazi University, for their valuable help in determining the point of research, advices during the fieldwork and constructive guidance during the preparation and revision of this work.

I would like to express my gratitude to Mr. Mahmoud Khairy (structural geologist, faculty of science, department of geology, Alexandria University) for his logistic help in the preparation of the thin sections. Thanks also must be extended to the Nuclear Materials Authority of Egypt. Thanks also to Mr. Waleed Al Khufify for photographing thin sections.

I am very grateful to the staff members in the Department of Earth Sciences, Benghazi University, Especially Dr. Fars Fathi, Dr. Fathi Salloum and Dr. Muftah Al Shwihdy for their cooperation and assistance during the whole period of my study.

Finally, I am deeply indebted to my family, especially my late mother and to my father for their love, support and encourage during the years of study, also the thanks extends to all family members.

Thanks to my friends Mohammed Al Riaydh, Al Moatasim Al Masmary, Hassn Al Shafi, Ahmed Al Amin, and Mohamed Najib

CONTENTS

CHAPTER III

CHAPTER IV

LIST OF FIGURES

LIST OF TABLES

ABSTRACT

This work discusses the petrographical and geochemical characteristics of the siliceous deposits (chert) at Al Jabal Al Akhdar, NE, Libya. These deposits exist in Al Athrun, Apollonia, Darnah and Wadi Qattarah formations. Petrographically, the siliceous materials in the chert samples are radiolarian shells in Al Athrun Formation, sponge spicules and microcrystalline quartz in Apollonia and Darnah formations, and microcrystalline quartz in Wadi Al Qattarah Formation, which support the biogenic origin of the cherts (except for Wadi Al Qattarah Formation). Geochemically, the studied cherts display ratios of seawater and biogenic silica almost similar to Si/(Si+Fe+Al+Ca) (0.59-0.96), Ge/Si (0.41-0.65), Hf/Ta (1.32-2.43), Zr/Ta (117.14-357.96), and Zr/Hf (56.55-161.23). This interpretation is further supported by the discrimination diagrams. The studied cherts fall under the non-hydrothermal type. The V/Cr, Ni/Co and U/Th ratios indicate that the studied formations were deposited under oxic conditions. Climatic conditions of semi-humid prevailed during the deposition of the cherts. The presence of clay minerals in the cherts is supported by the low K_2O/Al_2O_3 ratio and the positive correlation between Al_2O_3 and $K_2O + Na_2O$. The main tectonic settings are C and D (active continental margin and passive margin, respectively).

CHAPTER I

1-Introduction

1.1 General statement

Cherts are fine-grained siliceous chemical sedimentary rocks made up of interlocking microquartz crystals and chalcedony “radiating silica fibers few tens to hundreds of microns long”. Chert form either as primary sediments or by diagenetic processes Gary (2009). On the floors of seas and lakes the siliceous microfossil skeletons may accumulate to form a siliceous ooze “Radiolarians ooze in deep marine or Diatomaceous ooze in lake or marine bodies”. Radiolarians are zooplankton (microscopic protists with a planktic lifestyle) diatoms are phytoplankton (free-floating protists). Upon consolidation these oozes form beds of chert. The opaline silica (opal is cryptocrystalline silica with water in the mineral structure) of the diatoms and radiolaria is metastable and recrystallises to chalcedony or microquartz Gary (2009). Cherts formed from oozes are often thin bedded with a layering caused by variations in the proportions of clay-sized material present. They are most common in deep-ocean environments. Diagenetic cherts are formed by the replacement of other mineral such as “calcite” by silica-rich fluid. The source of the silica is mainly biogenic from diatoms, radiolarians, silicoflagellates and siliceous sponges, in form of nodules, such as the dark flint nodules which are common within the Cretaceous Chalk, and as nodules and irregular layers within other limestones, Gary (2009). The dense internal structure of interlocking microquartz grains and fibers makes chert the hardest sedimentary rock. It breaks with a conchoidal fracture and can form fine shards when broken, a feature which made this rock very significant in the development of tools by early humans. Cherts display different colors in accordance to proportions of impurities, which in red in Jasper due to hematite inclusions, gray-dark gray in Flint due to organic impurities. The petrographical examination of chert under thin sections will provide valuble informations about its nature, any digenetic signature and crystalline nature such as radiating, or chalcedony or interlocking microquartz. chert reveal characteristic patterns of either radiating fibers in chalcedony or completely interlocking microquartz grains, Gary (2009).

1. 2 Location of the study area

The study area located in northeast of Libya in the northern part of Cyrenaica, in a tectonic provinces called Al Jabal al Akhdar (figure.1.1).

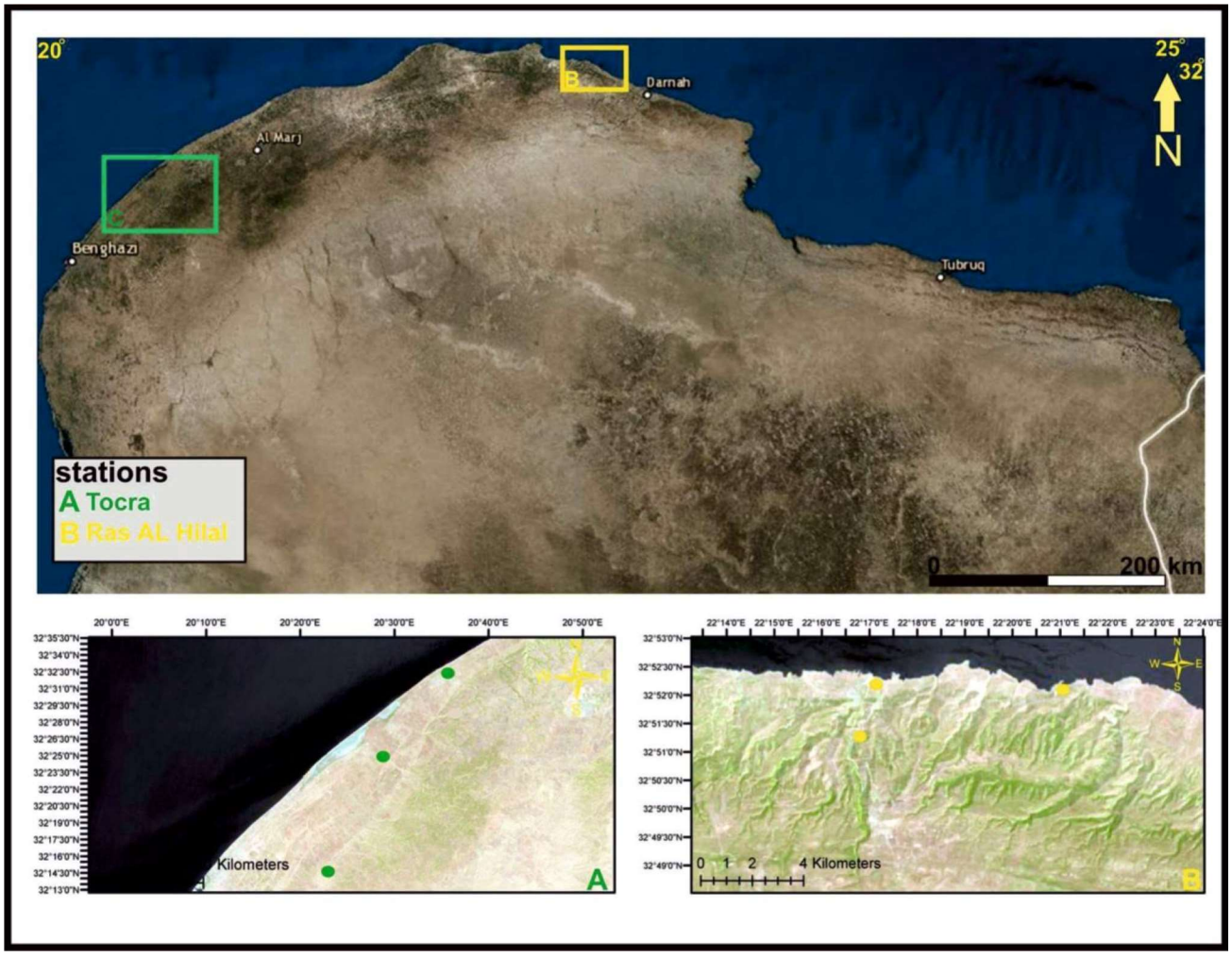

Fig.1.1. location map of Al Jabal al Akhdar shows the three studied areas

1.2.1. East Al Jabal al Akhdar (Ras Al Hilal area)

Three localities have been visited and sampled in Ras Al Hilal area, (Fig1,2) these are: -

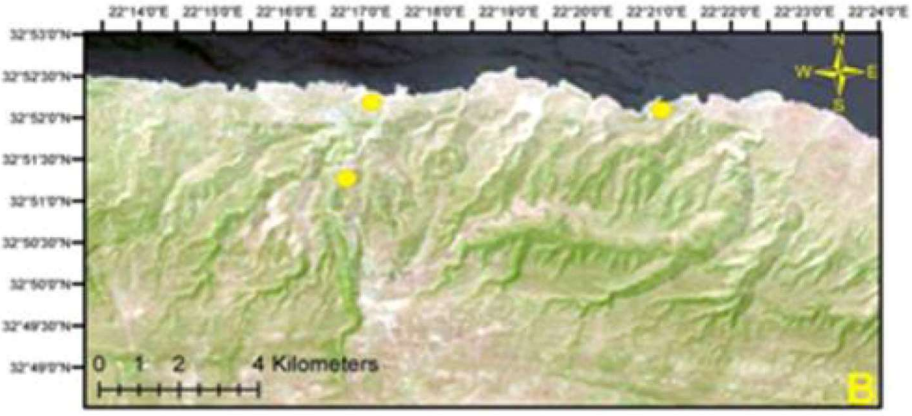

Fig. 1.2: satellite image of Ras Al Hilal area showing three localities

1) **locality no. 1:** Mouth of Wadi al Athrun (32^0 52' 16.7" N and 022^0 17' 03.9" E)

AL-Athrun Formation close to mouth of Wadi al Athrun along the coast where the most pronounced deformed Upper cretaceous beds of Al Athrun Formation.(Fig.1.3).

Fig.1. 3: General view of Athrun outcrop at locality (1) at mouth of Wadi al Athrun (looking E)

2) **locality no. 2:** (32^0 51' 49.0" N, 022^0 16' 50.5 "E) Wadi al Athrun village.

Apollonia Formation at Wadi al Athrun close to Athrun village where the deformed lower-Middle Eocene beds with two short unconformity surfaces. (Fig1.4)

Fig.1.4**:** General view of Apollonia formation at Wadi Al Athrun village (looking E). (Note: slump above the second uncoformtiy of El Hwat, 2008**)**.

Locality no. 3: pyramid section (32^0 52' 03.7" N, 022^0 20' 50.5" E).

Lower- Middle Eocene Apollonia Formation at it is type locality" pyramid section" at latitude and longitude (Fig.1.5).

Fig. 1.5: General view of rhythmic Apollonia Formation at pyramid section along Al Athrun-Karsa Road-Cut (looking E)

1.2.2 West Al Jabal al Akhdare Tocra area

Three localities have been sampled in this area: -

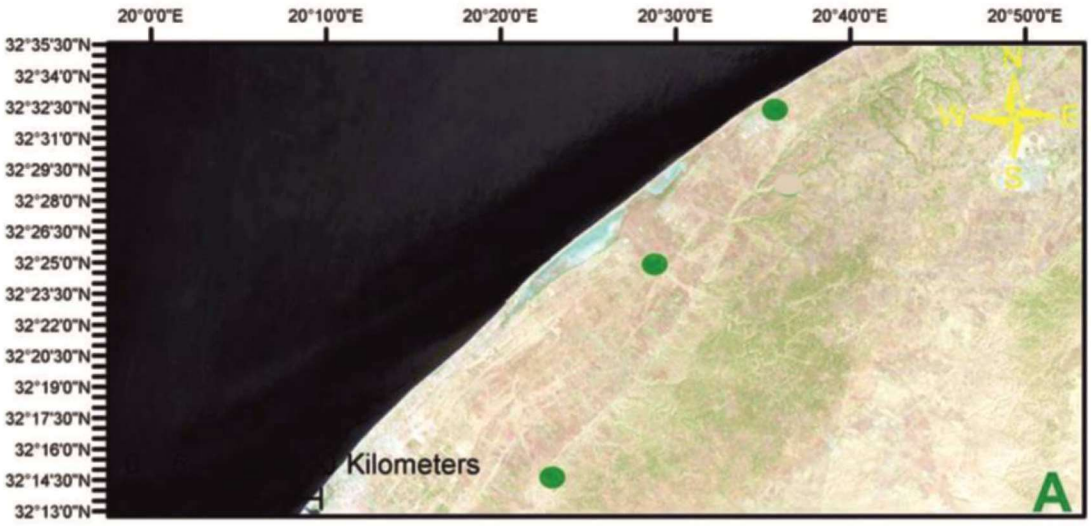

Fig. 1.6: satellite image of Tocra area

1) **locality no**. 1: Tocra City (32^0 31' 59.7" N, 020^0 34' 22.7" E)

The Apollonia Formation is exposed as tilted bedded yielded irregular small chert nodules (Fig. 1,7)

Fig. 1.7: General view of Apollonia Formation at Tocra City (looking W)

2) **locality no. 2**: Bersas- Al Hamada road cut (32^0 25' 12.8" N, 020^0 32' 01.4" E). cut south to Bersas village where Middle-Uppr Eocene limestone yielded chert nodules of Darnah Formation is well exposed. (Fig1.8)

Fig.1.8: Close –up view shows irregular Chert nodule in Darnah Formation, at the base of Barsas Al Hamada roadcut.

3) **locality no. 3**: Daryanh-Abyar road cut (32^0 16' 38.4" N, 020^0 29' 21.5" E) Which represents abandoned gypsum quarry of cement factory where Messinnian Wadi al Qattarah Formation is exposed. (Fig.1.9).

Fig. 1.9: General view of Wadi al Qattarah Formation at Gypsum Quarry Daryanh-Abyar road cut (looking N)

1.3 Regional geology

Al Jabal al Akhdar Uplift

The area of Al Jabal al Akhdar Uplift (the Green Mountain), the northern, mountainous part of Cyrenaica has a complicated yet intelligible geological history (Fig.1.10). It displays a Late Cretaceous, gently south-vergent folding event, followed by an isostatic rise, creating a gentle unconfonnity between the Maastrichtian and the Paleocene and Eocene. The Upper Cretaceous section is exposed in the axes of two prominent anticlinal structures forming the Jardas al Abid and Al Majahir inliers. There is also a known section of deformed thick Upper Jurassic and Lower Cretaceous syn-rift sediments, overlying an inferred Triassic section.

The southern and eastern boundaries of Al Jabal al Akhdar are defined (and genetically linked to) segments of the Hilal and Bomba shear zones. The northern boundary is partly formed by the Binghazi Shear Zone and the edge of deformation, which parallels the coastline just offshore, (El-Arnauti; et al, 2008). For more details regarding the structural of NE part of Libya see El-Arnauti; et al., (2008).

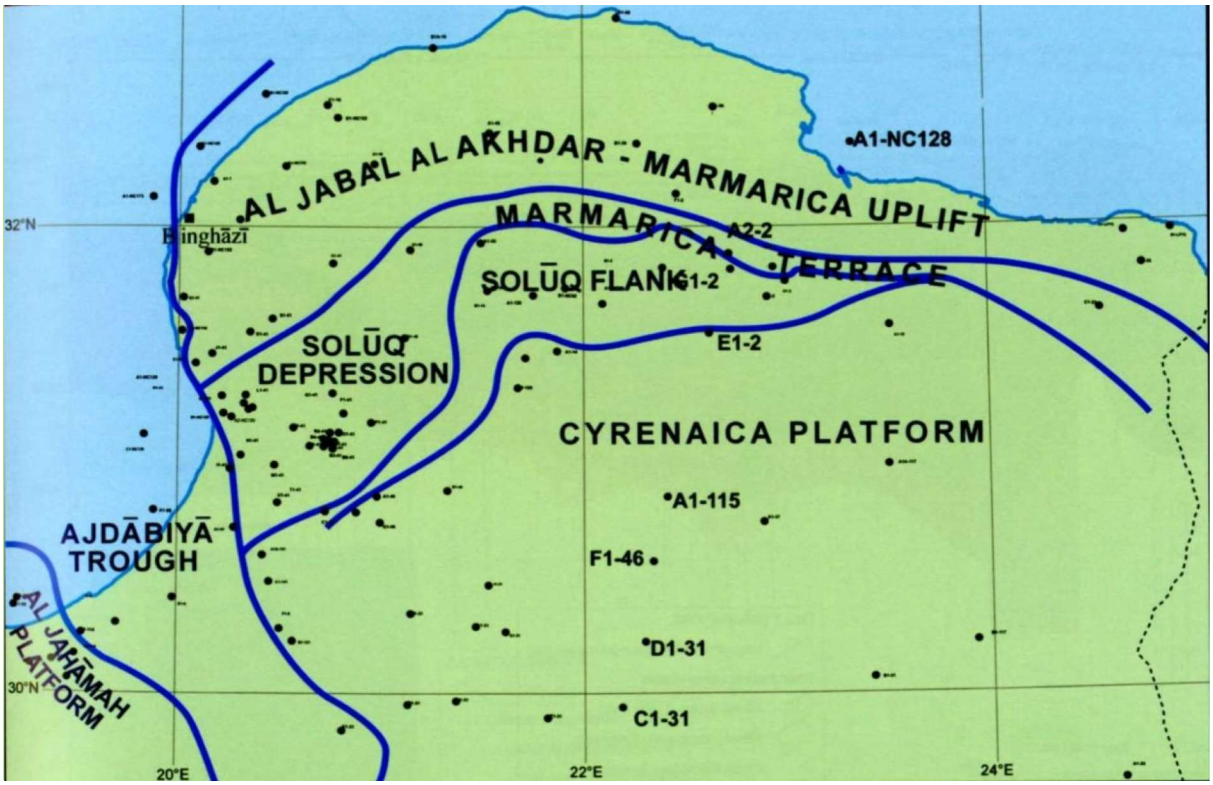

Fig. 1.10: Map of northern part of Libya, (after El-Arnauti et al., 2008).

1.4. Stratigraphic of the studied sections

Al Jabal al Akhdar generally consists of seventeen formal rock units (Fig.1.11) in response to the three structural stage of that defined by (Rohlich 1978), which are Lower stage (Cenomanian-Coniacian), Middle stage (Campanain- Landenian), Upper stage (Ypresian- Middle Miocene). The latter one subdivided further into five substages each resembling sedimentary cycle and separated from each other by unconformity surface.

The lower structural stage considered as the strongest one in terms of deformational effect "folding, joints, faults". Latter on, five stages have been re-established by Rohlich 1980.

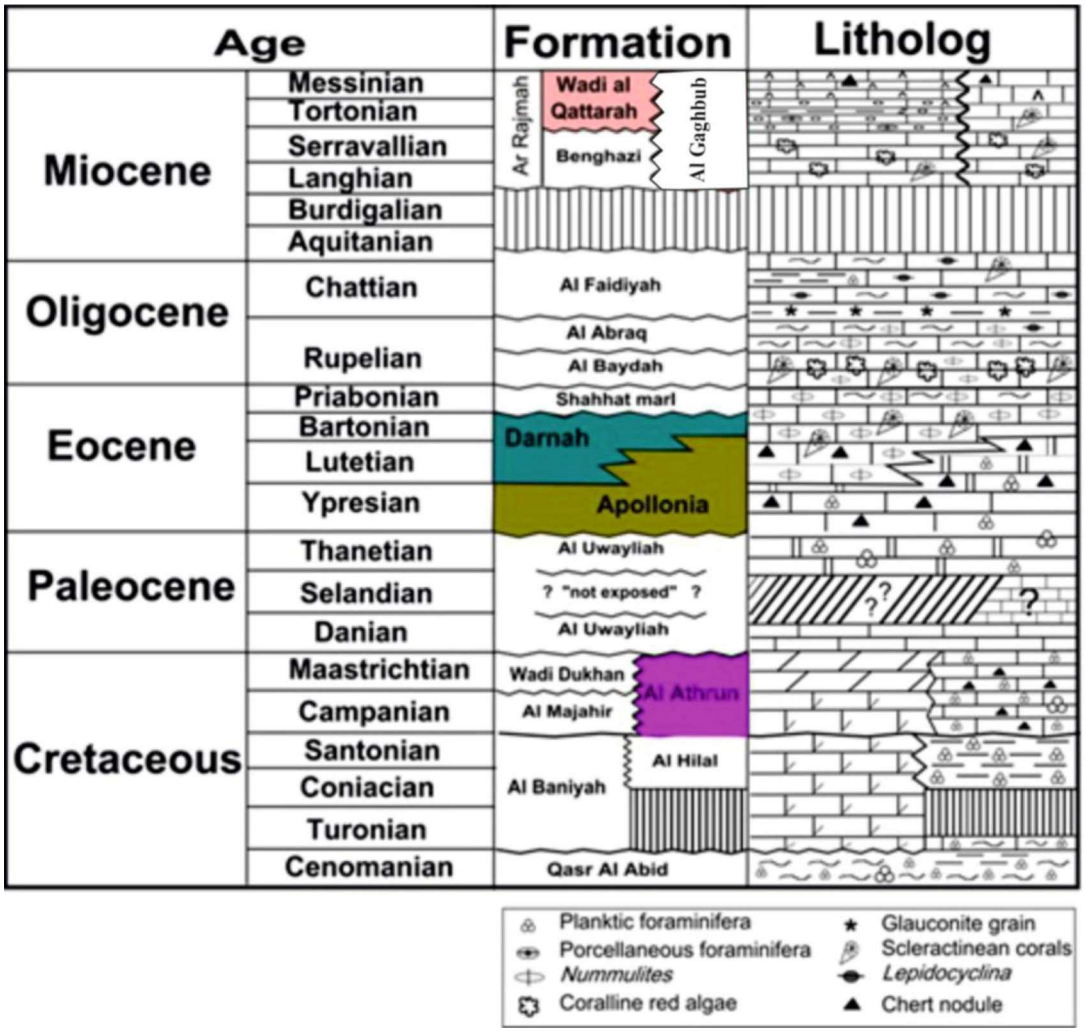

Fig. 1.11: A stratigraphic summary of the exposed formations in Cyrenaica region (after, Muftah et al., 2015). (Note: The highlighted formations are used in this study).

The targeted localities represent four stratigraphic rock units; these are from oldest to youngest (Fig.1.11):

1) Late Cretaceous (Athrun Formation)
2) Early – Middle Eocene (Apollonia Formation)
3) Middle-Late Eocene (Darnah Formation)
4) Late Miocene (Wadi al Qattarah Formation)

1.5 Objective of this study

1. Determine the digenetic history affecting the chert based on petrographically examinations.
2. Determine the environmental of depositions, with paleo-oxygenation level and peleoclimate condation.
3. Integrate the outcome of these methods to give possible origin of each chert.
4. Investigate the tectonic setting of the studied cherts.

1.6 Methodology: The methods used herein are outlined below:

1.6.1 Sampling

Fresh cherts (nodules and bands) as well as the hosted limestones were collected from Athrun, Apollonia, Darnah and Wadi Al Qattarah formations.

1.6.2 Thin sections petrography preparation:

The collected samples were examined under binocular microscope; the cherts and the hard limestone samples were chosen for thin section, from which 21 thin sections were prepared for all studied localities at the University of Alexandria, Geological Laboratory in Alexandria – Egypt, Generally, due to the very consolidated nature of the collected rock samples (mostly cherts with some hard limestones), the sediments are impregnated with bonding cement (Epoxy), and a blue powder dye is added in some cases before section in order to facilitate recognition of porosity from cement. The thin-section preparation technique involves the following steps:

1) Sawing and grinding the sample to reach slice measures of 30x22x3mm, grind the smoothest side with 80-100 mesh abrasive on the course lap wheel, followed by 320 and 600 mesh abrasives respectively.

2) Mounting the slice by using thin layer of raw Epoxy and cook.

1.6.3. Photography:

Colored photomicrographs for the selected petrographic slides have been taken using an Olympus petrographic microscope (BX41) with attached photographic system (DP12).

1.6.4 Geochemical Analytical techniques

1) Analysis of major oxides

2) Analysis of trace elements

3) Analysis of silicon isotopes

4) Analysis of total organic carbon (TOC)

1) Analysis of major oxides

Powder samples were mixed with a lithium tetraborate powder in a platinum crucible. The mixture was melted and formed pellets, which underwent high temperature (>1000oC) glass fusion for 2 h. The major oxides were determined using x-ray fluorescence (XRF) at the ALS Chemex (Guangzhou) Co., Ltd. The standard reference materials (SARM-45) were analyzed together with unknown samples, and the obtained precision was better than 5% (Fan et al., 2014). The analysis was analyzed at the Nuclear Materials authority of Egypt.

2) Analysis of trace elements

The trace elements were determined by inductively coupled plasma mass spectrometry (ICP-MS) at the Nuclear Materials authority of Egypt. Powder samples (50 mg) were digested in a PTFE bomb using ultrapure HF and HNO3 acids under pressure at high temperature (190oC) for 12 h.

After complete digestion and HF-HNO3 evaporation, the samples were diluted in 3% HNO3 using a quantitative Rh internal standard solution. The clear solution was analyzed for trace elements and rare earth elements using ICP-MS (Qi et al., 2000). During the analytical processes, the standard reference materials (AGV-2 and AMH-1) were measured together with the samples at REE accuracy of 3% and Ge accuracy of 10%. Our REE and Ge results are consistent with previous data reported by Raczek et al., (2001).

3) Analysis of silicon isotopes

The analysis was analyzed at the Nuclear Materials authority of Egypt. About 0.5 mg of sample material was mixed with sodium hydroxide monohydrate (NaOH·xH2O) and placed into a Parr bomb at 200°C for two nights. Multiple digestion steps were applied if necessary, where the residual solid was separated from the supernatant. The silicon was extracted with Biorad AG50-X8 cation exchange resin. After purification, the silicon concentration was determined on a Varian 720-ES ICP-OES to exclude any loss. Only samples with N97% yields were accepted for isotope analyses. Silicon isotopes were measured on a ThermoFinnigan Neptune MC-ICPMS instrument equipped with a Cetac Aridus I desolvating nebulizer at the VU University Amsterdam. Analytical runs were performed in medium-resolution mode (Rpower = 2500).

A typical analytical sequence was composed of blank, standard-I, blank, sample, blank, standard-II, etc. Silicon isotope data are reported in the delta notation relative to NIST RM8546 (NBS-28) according to Albarede et al., (2004):

$$\delta^{29}Si = \frac{\left(^{29}Si/^{28}Si\right)_{sample}}{\left(\left(^{29}Si/^{28}Si\right)^{0.5}_{std-I} \cdot \left(^{29}Si/^{28}Si\right)^{0.5}_{std-II}\right) - 1} \cdot 1000 \qquad (1)$$

$$\delta^{30}Si = \frac{\left(^{30}Si/^{28}Si\right)_{sample}}{\left(\left(^{30}Si/^{28}Si\right)^{0.5}_{std-I} \cdot \left(^{30}Si/^{28}Si\right)^{0.5}_{std-II}\right) - 1} \cdot 1000 \qquad (2)$$

The 28Si blank was between 20 and 60 mV. The precision and accuracy for the total silicon isotope procedure was assessed with USGS international standards BHVO-2 (n = 14) and AGV-2 (n = 12) which yielded δ30Si values of−0.27± 0.14‰ and−0.13± 0.16‰ (2 s.d.), respectively. These values are in good agreement with data from Zambardi and Poitrasson (2011). Analyses of an in-house standard solution (Silicon Single Crystal), which tests the precision and accuracy of the Neptune instrument, yielded an average δ30Si of -2.54 ± 0.20‰ (2 s.d., n=18). This compares well with data for this standard reported elsewhere (Kempl et al., 2013). Based on the two international standards and the in house standard, we adopt a precision for the total procedure for δ30Si of ±0.20‰ (2 s.d.), valid at a measurement intensity for 28Si of 4–6 V. Because carbonaceous matter and sulfur can influence silicon isotope measurements by MC-ICPMS (van den Boorn et al., 2009), a set of sulfur and organic-free samples was prepared for comparative analysis. About 20 mg of sample material was treated in a routine for thermogravitational analysis (TGA) in the temperature range from 20°C to 900°C, with a heating rate of 10°C min-1 and a gas flow of a synthetic air mixture of 40 ml min-1. The weight losses were recorded.

4) Analysis of total organic carbon (TOC)

The same procedures used by El-Shafeiy et al., (2014) are also used here. The homogenized samples were measured for TOC contents (wt% whole rock) in the laboratories of Strato Chem in Egypt. The rock material was ground and thereafter weighed into a Pyrex beaker and reacted with HCl to dissolve any inorganic carbon in the samples. The samples were then transferred onto glass microfiber filter papers using a Millipore filter apparatus. The filters containing the samples were combusted in a LECO C230 or LECO EC-160 12 furnace, where the resulting CO2 was quantitatively measured using an infrared detector. For Rock Eval measurements, the ground rock material was placed into an auto-sampler crucible. During isothermal heating (300ºC), S1 free hydrocarbons were volatilized and detected by a flame ionization detector. A temperature increase to 600ºC caused the release of additional hydrocarbons (S2) and simulated the pyrolytic degradation of kerogen in the rock. This is roughly equivalent to the hydrocarbon potential of the rock and after being divided by the TOC is expressed as the hydrogen index (HI). The carbon dioxide that was released up to approximately 400ºC is reported in milligrams per gram of rock (S3).

1.6.5. Picking

Foraminifers are prepared according to standard micropaleontological techniques, in which samples are disaggregated by soaking in washing soda solution in accordance to the chalky sediment nature. This is followed by washing over a 63µm sieve to remove the silt and clay fractions. Samples are dried and picked up.

1.7. Previous studies

It is worthy to note that the published data on the cherts at Al Jabal al Akhdar are very insufficient. Generally, everywhere, studies on the cherts are very rare compared to those on the limestones. Very limited effort has been given to the cherts at Al Jabal al Akhdar. In this respect the detailed characteristics of their formation are given, especially in the absence of many published works on the subject.

Amrouni et la., (2016) studied the silicification in the Cyrenaican Miocene carbonate-evaporite sequence, NE Libya. They found that in the Ar Rajmah Group, the silica is very common in the ramp crest oolitic grainstone facies and peritidal microbialite facies, but rare in the subtidal red algal and bioclastic packstone facies. The silica commonly occurs as chert nodules of reddish-bluish light gray color in the ramp-crest and peritidal facies and is whitish light gray color in the subtidal facies. In addition, the silica forms in up to 20 cm thick, discontinuous layers in the porous mixed microbial-oolitic grainstone facies. In thin section, the silica forms as disseminated silica, microquartz, and chalcedonic quartz. It replaces matrix, grains, cements, and even forms authigenic fan-shaped chalcedonic cement that filled up pore spaces. In the paragenetic sequence of the Cyrenaican Miocene, silicification always comes as the last replacement process after dolomitization, dedolomitization, and gypsum replacement. All studied silica samples are length slow while the gypsum plate is inserted in the XPL position. A study of all samples did not reveal any evidence of a biogenic origin for the silica. In the Cyrenaican Miocene carbonate-evaporite sequence, the diagenetic silica occurrence and distribution are strongly facies controlled and have no correlation with the sequence stratigraphic surfaces or systems tracts. Also, the silica originated from continental weathering rather than being biological, as evidenced by the strong direct proportional ngeochemical relationship between the silicon and aluminum, as well as the petrographic analysis.

CHAPTER II

2-Sedimentology and petrography

Siliceous sediment is occurred in Al Jabal al Akhdar at four exposed rock units, these are: 1) Al Athrun Formation (Upper Cretaceous) at the mouth of Wadi al Athrun; 2) Apollonia Formation (Lower-Middle Eocene) which is exposed in three localities, a) Wadi Athrun at Athrun village, b) pyramid section at Athrun-Karsa roadcut, and c) Tocra city; 3) Darnah Formation (Middle-Upper Eocene) which is exposed in Bersas-Al Hamada road cut, in the vicinity of Bersas village; 4) Wadi Qattarh Formation (Upper Miocene) which is exposed along the gypsum quarry along Dryanah-Abyar road cut. All of these formations are well exposed in the study area, and are containing different types of cherts (in terms of shape, color and chemical composition), all of these characteristic will be analyzed petrographically in this chapter and geochemically in the coming chapter. The cherts in each formation will be studied petrographically under Plane-Polarized light (PPL) and under crossed-Nicols Polarized light (XPL).

2.1 Petrographic and paleontologic analyses of cherts and hosting limestones:

The Cherts-bearing Formations of Al Jabal al Akhdar are addressed in this study from oldest to youngest as follows:

2.1.1 Al Athrun Formation (Late Cretaceous):

The name of Al Athrun Formation is adopted for the Al Athrun Limestone as defined by Barr and Hammuda (1971) for the Upper Cretaceous chalky white limestone in the Wadi al Athrun- Marsa al Hilal costal area of northern Cyrenaica. The type section is located near the mouth of Wadi al Athrun where it derives its name. The Formation is exposed along Ras al Hilal- Athrun sea cliffs in the eastern part of the area, and in some deeply cut wadis such as Wadi al Qalah as documented by Barr and Hammuda (1971) as well as El-Mehaghag and Muftah (1996). Close to The famous slumped section at the mouth of Wadi Athrun of El-Hawat and Shelmani (1993), the small section (12m thick sequence) of Upper Cretaceous Al Athrun Formation has been subjected to this study.

AL-Athrun Formation consists of tan, white, microcrystalline to fine grained, thin bedded, limestone with thin discontinuous banded and nodules of grayish brown with whitish external appearance cherts. An unconformable surface with the overlying Apollonia Formation (Early Eocene) is well exposed in Wadi Al Athrun section. The Al Athrun Formation yields abundant foraminifers containing a high percentage of planktic foraminifers (Barr, 1972; Barr and Hammuda 1971) and calcareous nannofossils (Hay (1968); El-Mehaghag and Muftah 1996). Radiolaria and *Inoceramus*-prisms are also being recognized. According to the common occurrence of foraminifers the Al Athrun Formation ranges in age from the Late Coniacian to the Late Maastrichtian (Barr and Hammuda (1971), however, the age is confined to Late Campanian based on calcareous nannofossils as suggested by El Mehaghag and El Mehdawi (2006) form Wadi al Athrun section.

The Al Athrun cherts are the oldest exposed chert nodules in the Al Jabal al Akhdar, they are usually small in size (≈10 cm). The studied of Al Athrun Formation with common cherts in study area was located at the mouth of Wadi Al Athrun (Fig. 2.1)

Fig 2.1: A view of chert nodules in Al Athrun Formation, at the mouth of Wadi Al Athrun.

This exposed section made up with 12m thick sequence. It composes of limestone, white color, wackestone grading to packstone texture, very chalky, medium hard, becoming very hard upward, thick bedded with common *Inoceramus*-prisms and planktic foraminifers. It yields chert nodules up to 35cm along the long axis (Fig 2.1). At this locality, three chert levels have been noted, which was deposited as thin individual nodules becomes nearly connected nodule in a discontinuous band-like at the lower most part (Fig. 2.2). It is characterized by milky white color on surface becoming dark brown due to inclusions with organic matter, discoidal-flattened, compressed and extensively cracked and fragmented due to tectonism as evidenced by folding and extensive jointing (see Elamawy et al, 2011). At this locality, the presence of rare radiolarian tests in the Al Athrun cherts is strongly supporting the biogenic origin of this cherts (Fig. 2.6).

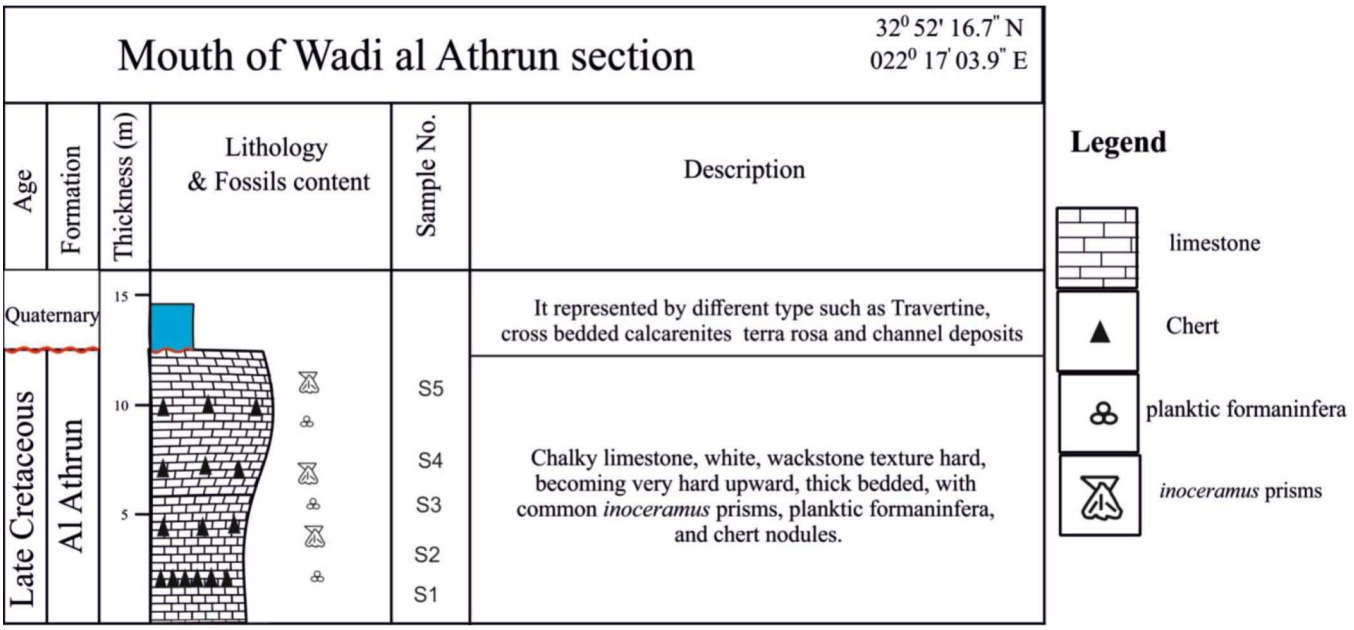

Fig. 2.2: Lithological column of the studied Al Athrun Formation at the mouth of Wadi Al Athrun.

Petrographically, the Athrun cherts at the mouth of Wadi Al Athrun contain high percentage of silicified Late Cretaceous planktic foraminifers such as *Globotruncana stuartiformis* and *Heterohelix globulosa* (Fig 2.3), *Rugoglobigerina rugosa* (Fig 2.4) as well as silicified walled elements of pelecypods called *Inoceramus*-prisms (Fig 2.5). However, the hosting (surrounding) limestone are made of wackestone grading to packstone at local places with common planktic foraminifers such as *Globigerinelloides* sp. and *Inoceramus*–prisms (Fig. 2.8)

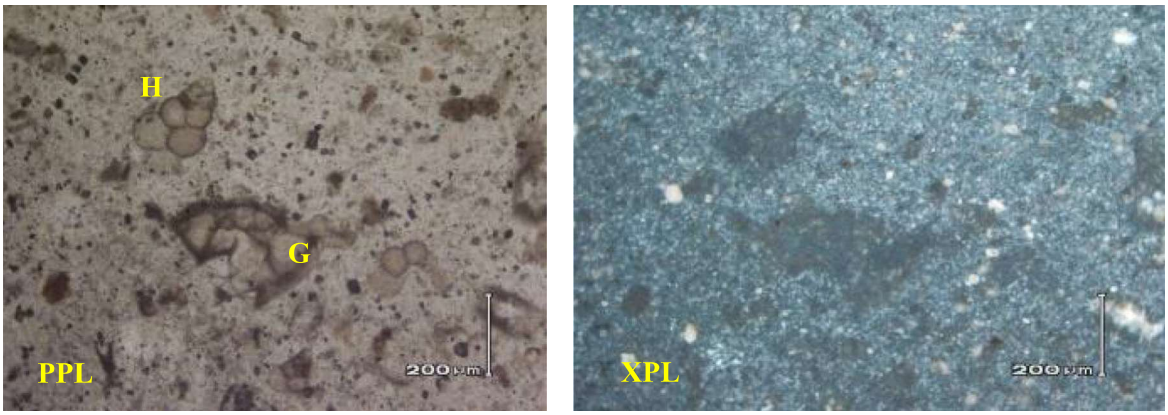

Fig. 2.3: Photomicrographs of Athrun cherts at the mouth of Wadi Al Athrun sections, showing *Globotruncana stuartiformis* and *Heterohelix globulosa*. Sample no. (1).

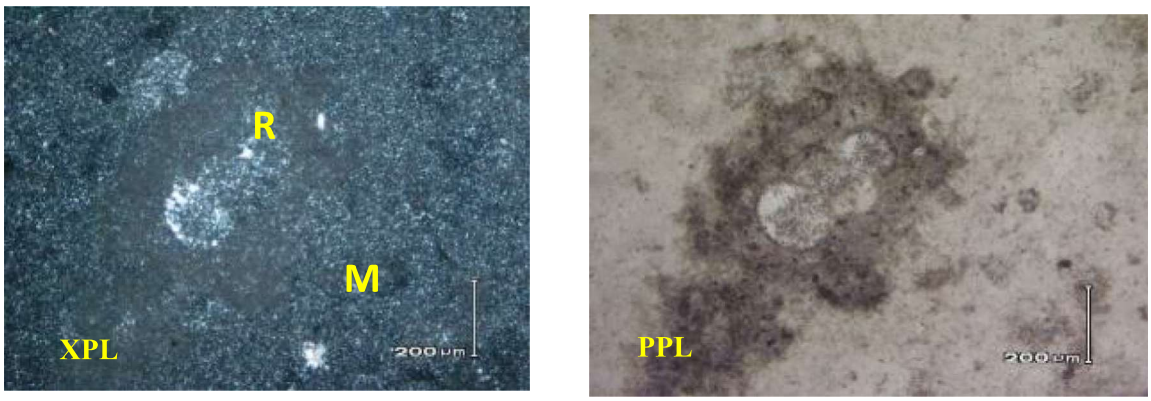

Fig 2.4: Photomicrographs of the Cretaceous Athrun Cherts at the mouth of Wadi al Athrun, showing the, (M) microcrystalline quartz groundmass containing silicified planktic foraminifers, (R) *Rugoglobigerina rugosa*. Sample no. (2).

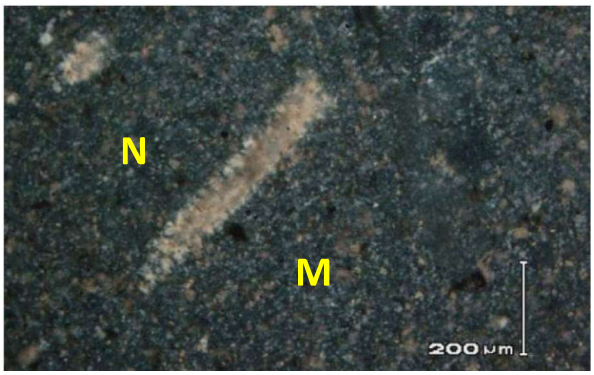

Fig 2.5: Photomicrograph of the Cretaceous Athrun Cherts at the mouth of Wadi Al Athrun, showing the (M) microcrystalline quartz groundmass containing silicified. (N) *Inoceramus*-Prism. Sample no. (2)

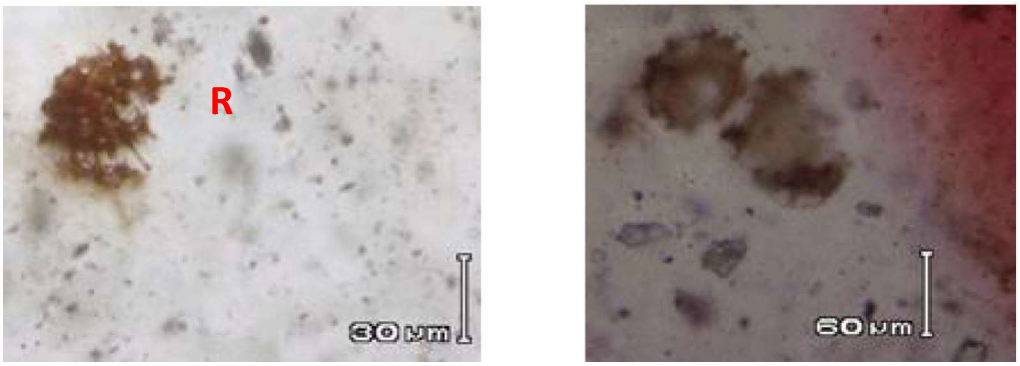

Fig 2.6: Photomicrographs of the Cretaceous Athrun Cherts at the mouth of Wadi al Athrun, showing radiolarian tests. Sample no. (4).

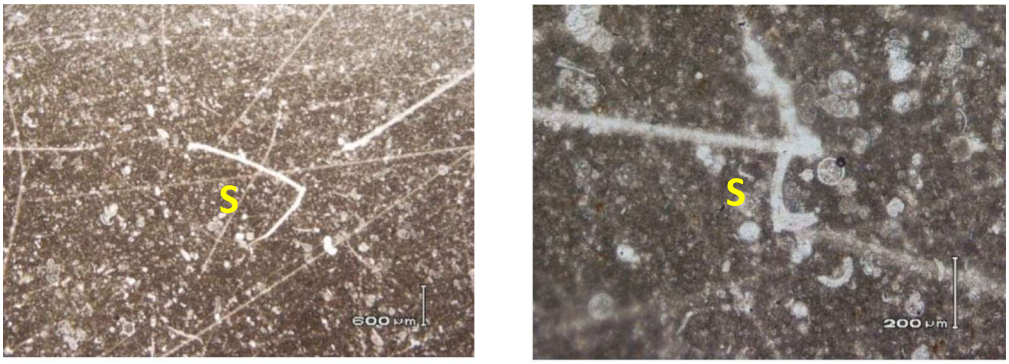

Fig 2.7: Photomicrographs of the Athrun planktic limestone at the mouth of Wadi al Athrun, showing (S) sponge spicules in micritic matrix. PPL, Sample no. (5).

Fig 2.8: Photomicrographs of the Athrun planktic limestone at the mouth of Wadi al Athrun, showing (G), *Globigerinelloides* sp. And (I), *Inoceramus*-prism in micritic matrix. PPL, Sample no. (5)

2.1.2 Apollonia Formation (Early-Middle Eocene)

The term Apollonia Formation was introduced by Pietersz (1968). The type locality is located along Al Athrun– Karsa roadcut called "Pyramid section". It shows only the uppermost part of Apollonia Formation with about 30m thick section. It largely consists of brownish cream, mudstone to wackestone textures, slightly chalky, medium bedded. An important feature of this formation is the occurrences of greyish to brownish chert nodules. Another unique feature of it is the bituminous smell produced by being struck with hammer (Rohlich, 1974). Apollonia Formation is dated as Early – Middle Eocene by Rohlich (1974); However, El Khoudary (1980) dated it as Middle Eocene age based on the recognized planktic foraminiferal biozones. On the other hand, El Mehaghag and El Mehdawi (2006) based on the recognized calcareous nannofossils assigned an age range of Late Paleocene to Early Eocene for the exposed Apollonia Formation at Wadi al Athrun section close to Athrun village (Fig. 2. 16).

Three localities of Apollonia Formation are sampled and studied petrographically with particular emphases to its contained cherts, these are:

2.1.2.1 Locality no. (1) called Pyramid Section:.

At this section Apollonia Formation made of 18m thick sequence of Limestone interbedded with marly limestone in a rhythmic pattern reflecting sea level fluctuation with occurrences of chert nodules at some levels. The limestone is characterized by greyish brown, medium-thick bedded, mudstone texture grading in parts to wackestone texture, with bituminous odor when struck by hammer, with common chert nodules of size range from few centimeters to more than 1m along long axis. However, the marly limestone interbeds, are white, mudstone texture, thin-medium bedded, with rare small-sized chert nodules, it is more often jointed locally, (Figs. 2.9-2.11).

The Apollonia cherts, are usually brownish in color, small in size of potato to ovoid shape, sometimes angular as seen in the type locality pyramid section (Fig. 2.11b).

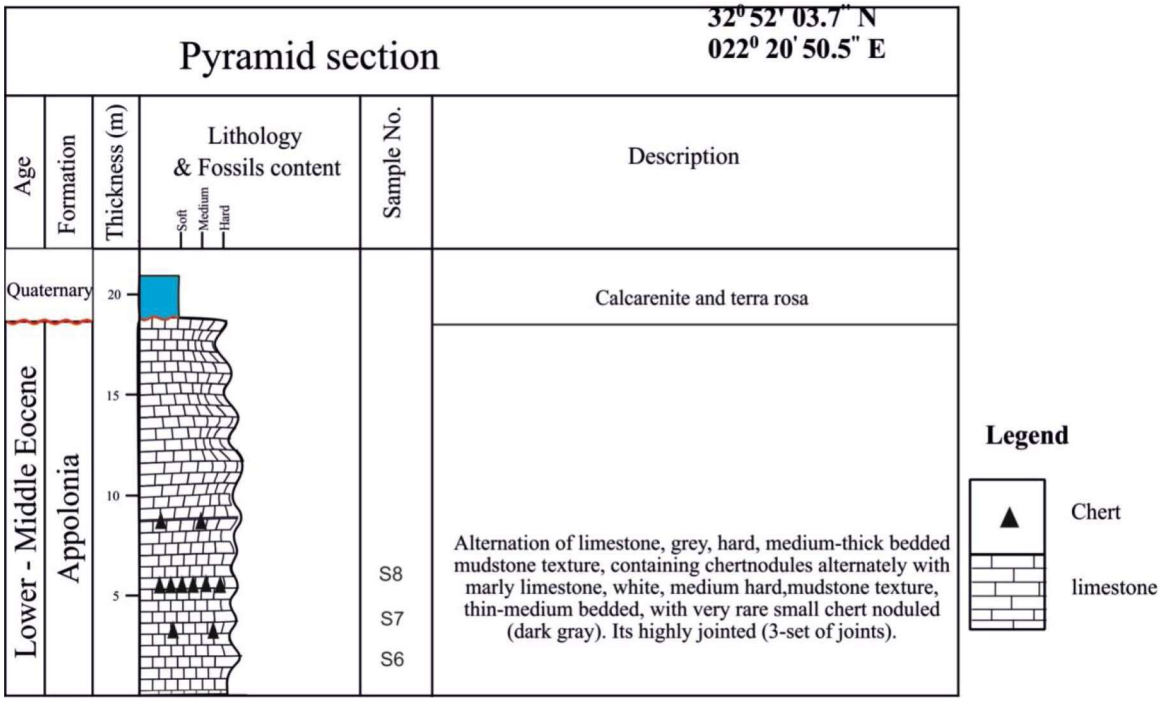

Fig. 2.9**:** Lithological column of Al Apollonia Formation at pyramid section, Al Jabal al Akhdar, Libya

A diagenetic origin of this chert as evidenced by the concentric growth pattern found in some nodules and the common diagenetic features of "silicified *Nummulites"* (El Amawy *et al.,* 2011; Muftah et al., 2015). The occurrence of the sponge spicules in the surrounding (hosting) limestones is supporting the biogenic source of the silica used in the chertification of these nodules (Figs. 2.12-2.13). The presence of sponge spicules in the Apollonia equivalent subsurface Ararah Formation (Starkie et al., 2007). At Well T1-41 in Sirt Basin together with *Nummulites* and local minor small benthic and planktic foraminifers supporting silica source at this level. Organic matter is reported in the small sized nodules of the thinner and white marly limestone intercalations (Fig. 2.14). However, only microcrystalline ground mass free of fossils is typified the cherts of the greyish brown, medium - thick bedded limestone (Figs. 2.15).

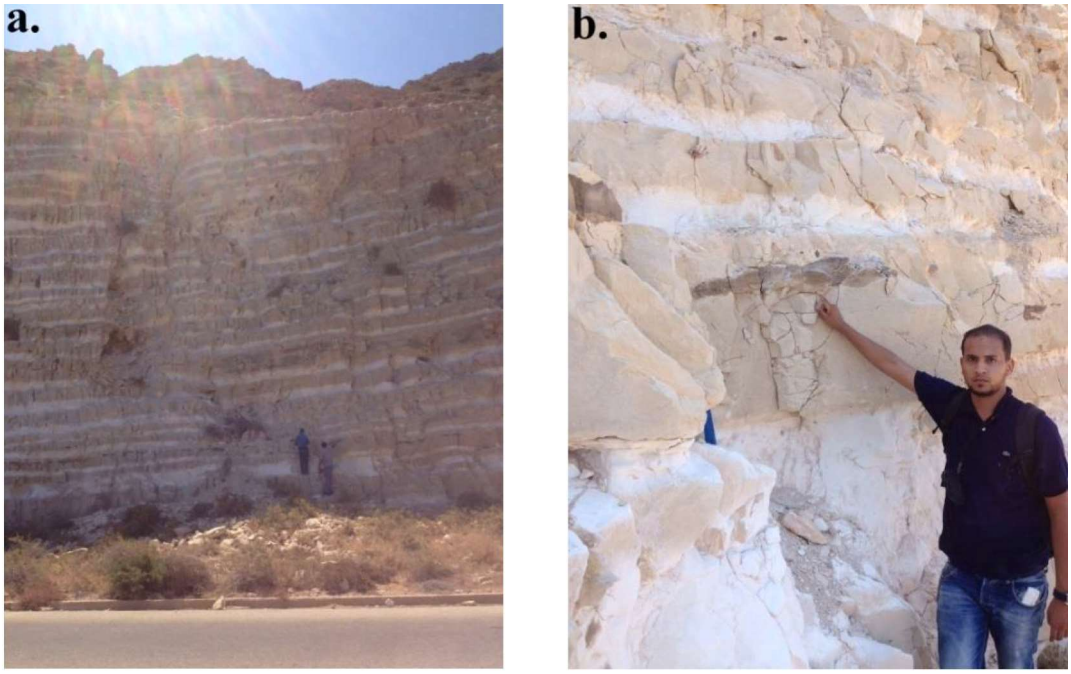

Fig. 2.10: Field photographs of Apollonia Formation show, a) alternation of beds; and b) cherts at the pyramid section along Al Athrun-Karsa road-cut.

Fig. 2.11**:** A rhythmic tabular beddings of Apollonia Formation showing cherts band-like at Pyramid section along Al Athrun-Karsa road-cut.

Fig 2.12: Photomicrograph of sponge spicule from Al Athrun limestone at pyramid section, Sample no. (6)

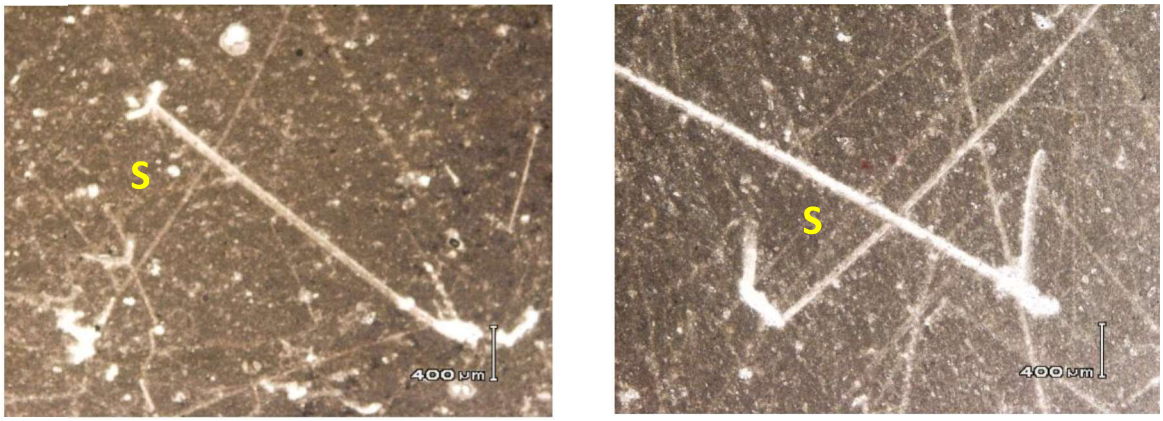

Fig. .2.13: photomicrographs show (S) sponge spicules embedded in the micritic matrix of Apollonia Formation from the pyramid section; PPL, Sample no. (6).

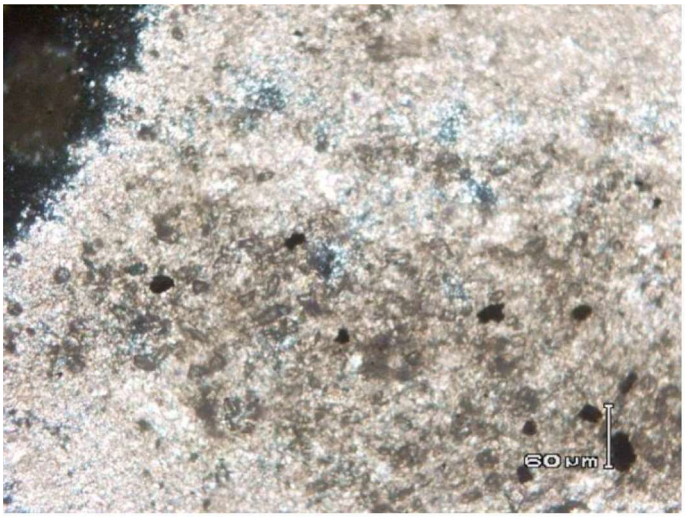

Fig. 2.14: photomicrograph of Apollonia Formation at pyramid section shows microcrystalline quartz with local organic-like material? XPL, Sample no. (7)

Chert nodules at this locality are finely crystalline texture replaces the existed planktic foraminiferal tests in most cases.

Fig. 2.15: Photomicrographs of Apollonia chert at the Pyramid section show microcrystalline quartz ground mass. PPL and XPL, Sample no. (8).

2.1.2.2 Locality no. (2) Wadi Al Athrun village Section:

Apollonia Formation at the well-known Wadi Al Athrun close to Al Athrun village, where, the most pronounced deformed beds and two unconformity surfaces of El Hawat and Shelmani (1993); El Hawat and Abdulsamad (2004); El Hawat et al., (2008). This section is well exposed where the angular unconformity between Athrun Formation and the Early Eocene Apollonia Formation as dated by Barr and Berggren, 1980); Hay, (1968); El Hawat and Shelmani (1993).

At this section the Cretaceous Athrun limestone is unconformbly overlain by Apollonia Formation, where two unconformaities (i.e. paraconformities) are recognized with Apollonia Formation by El-Hawat et al., (2008) (Fig. 2.16). The analyzed cherts in Apollonia limestone at this locality are collected from just below the lower unconformity -1. There is local slump structure can be observed in this section as well as the two local unconformity as indicated in (Figs.2.16 and 2.17).

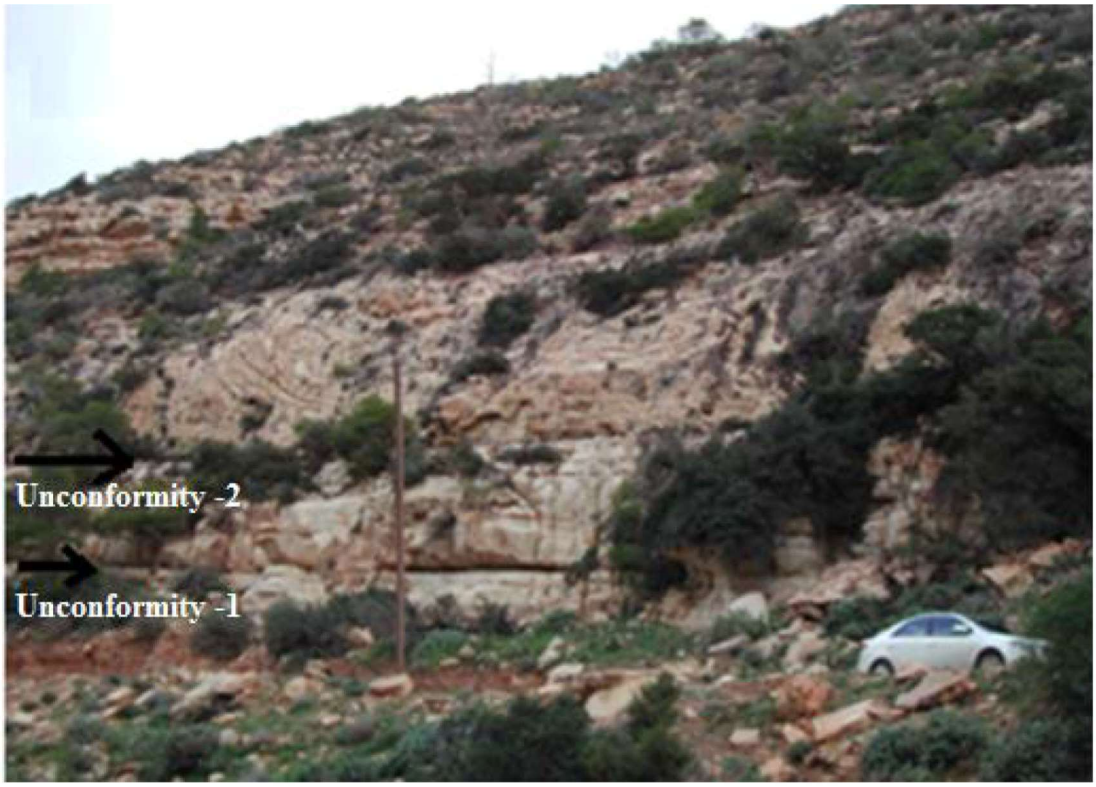

Fig.2 16: The Slump structure in Apollonia Formation at Wadi Al Athrun, section (Note the two unconformity surfaces indicated by arrows).

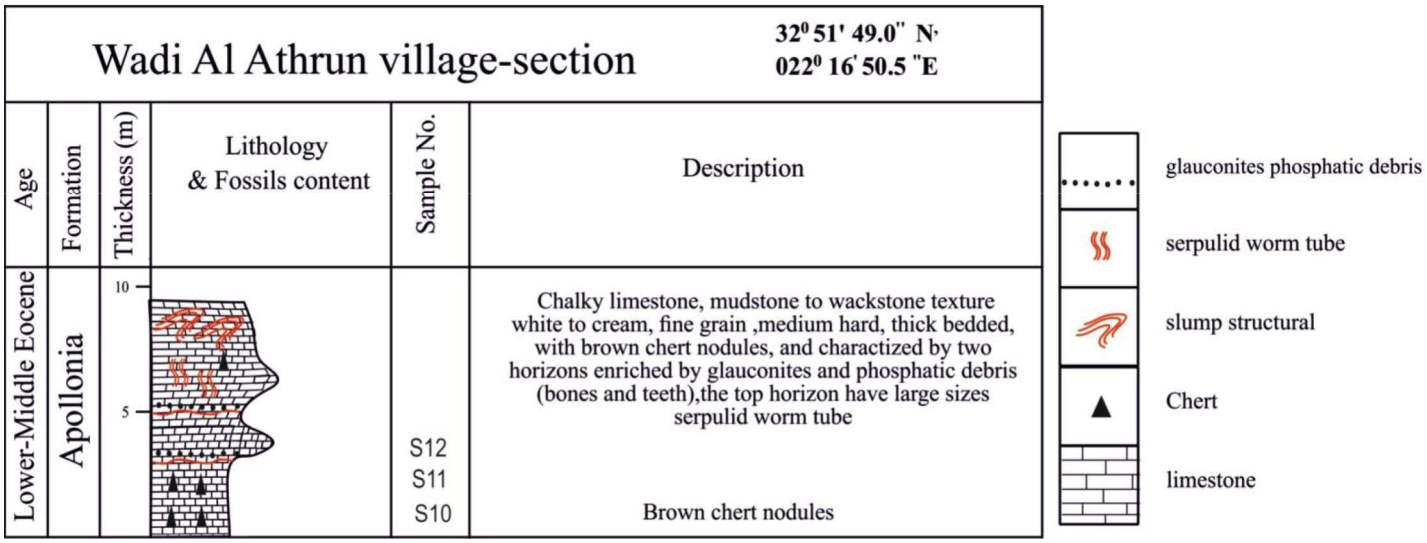

Fig.2.17: lithological column shows chert horizons, the two paraconformity surfaces and the slumped part of Al Apollonia Formation at Wadi Al Athrun section.

Fig. 2.18: Photomicrographs shows shark teeth (S) embedded in microcrystalline quartz groundmass from Apollonia Formation at Wadi Al Athrun. Sample no. (10).

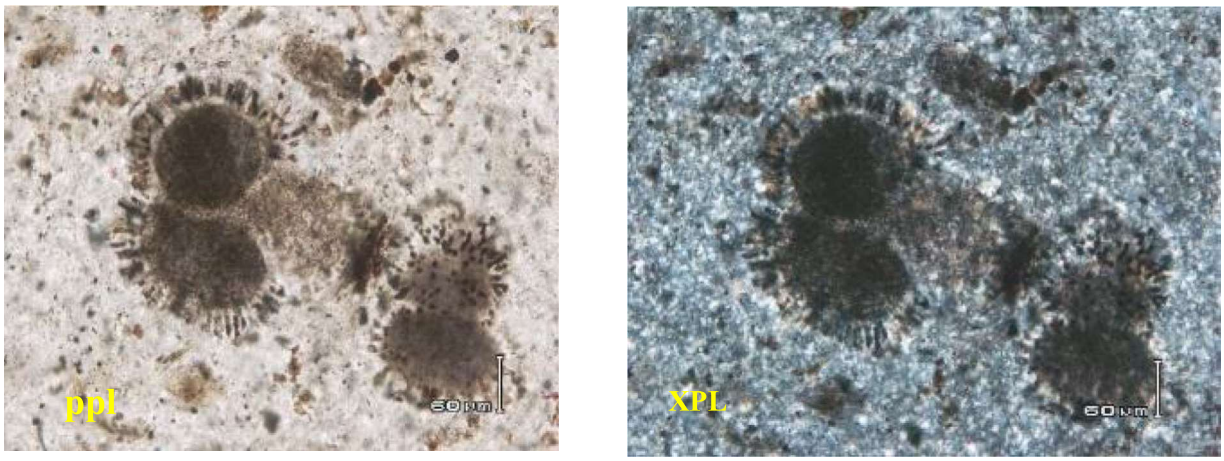

Fig. 2.19: Photomicrographs of microcrystalline quartz consist with thick walled globigerinids from Apollonia Formation at Wadi Al Athrun. Sample no. (10).

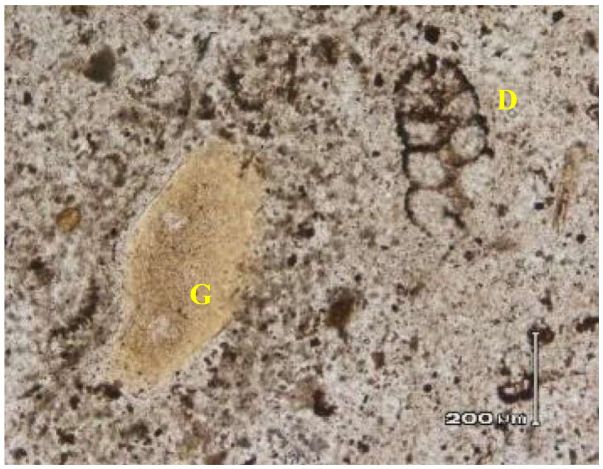

Fig. 2.20: Photomicrograph shows microcrystalline quartz groundmass containing *Gaudryina* sp.; (D) and phosphatic grain (G) form Apollonia Formation at Wadi Al Athrun section, PPL, Sample no. (10)

Fig. 2.21: Photomicrograph shows sponge spicules? from Apollonia Formation at Wadi Al Athrun village section, PPL, Sample no. (11)

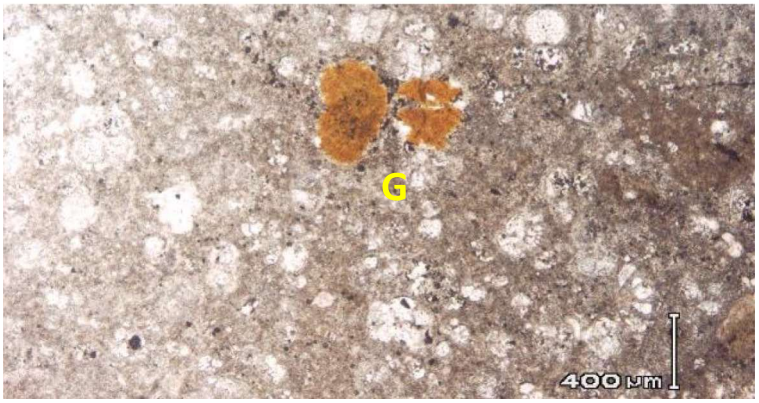

Fig. 2.22: Photomicrograph of globigerinids packstone texture of Apollonia Formation shows common planktonic foraminifera and sparse glauconitic grains (G) (orange). Sample no. (12).

2.1.2.3 Locality number 3 at Tocra City:

Apollonia Formation is exposed as patchy and intermittent tilted limestone containing rare chert nodules. Some scientists believed this limestone is Cretaceous in age such as Goudarzi, (1970); Klen (1974); Conant and Goudarzi, (1964) however, others considered it as Eocene including Pietersz (1968); Helmdach and El Khoudary, (1980) and El Mehaghag et al., (2008). Petrographically, the mudstone textured limestone of Apollonia Formation at this locality is containing some small sized chert nodules (range between 30- 50 cm), brown color, with no fossils observed (Figs. 2.23 and 2.24), however, the hosting limestone contains sponge spicule - like as seen in (Fig. 2.25).

Fig. 2.23: General view of patchy tilted occurrences of Apollonia Formation Tocra City

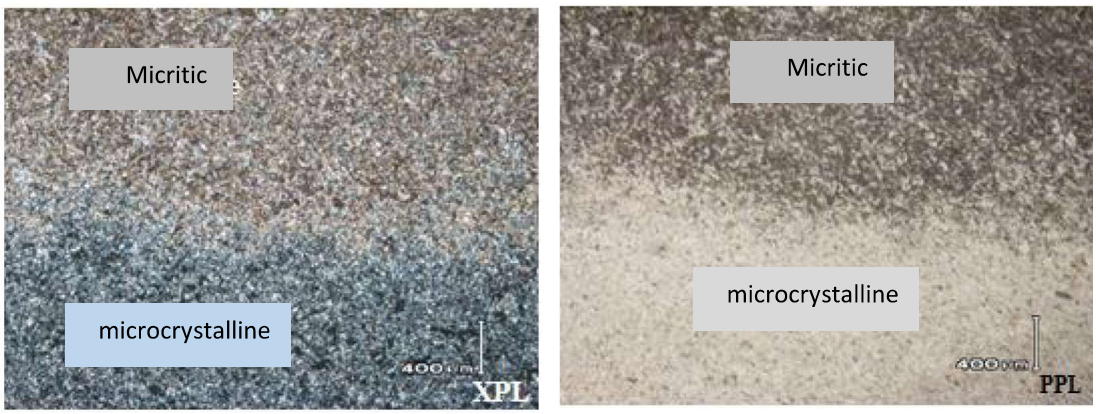

Fig. 2.24: Photomicrographs show chert limestone in contact from Apollonia Formation at Tocra city, sample no. (13)

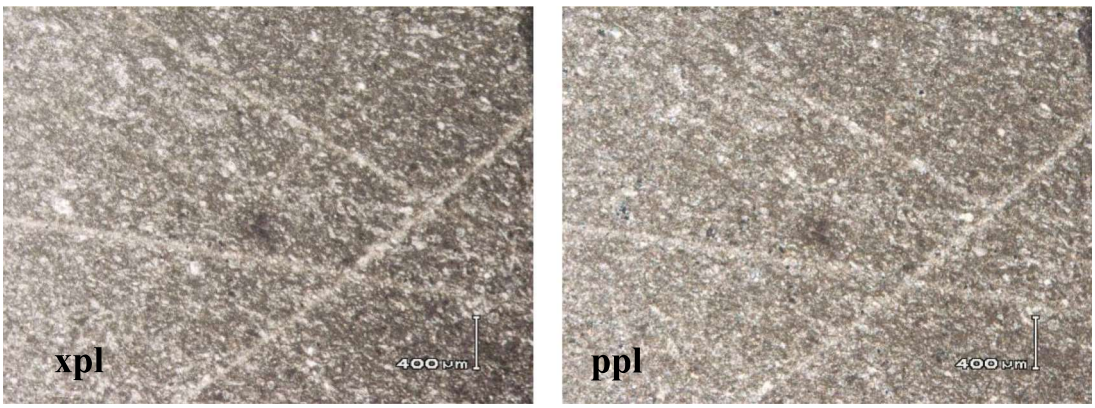

Fig. 2.25: Photomicrographs show sponge spicules-like from Apollonia Formation at Tocra. Sample no. (14).

2.1.3 Darnah Formation (Middle Eocene)

The term was introduced by Gregory (1911) as Derna limestone in northern Cyrenaica. He used this term for a prominent unit well exposed along the costal escarpment near Darnah city. The term Darnah Formation was given by (Klen, 1974; Rohlich, 1974; and Zert, 1974). It is extending from Wadi al Hassien east of Darnah in the East to the vicinity of Benina near Benghazi in the West. The lower boundary of the Darnah Formation is conformable with gradational contact from the underlying Apollonia Formation with inter fingering relationship between both formations which can been seen at local places as in Wadi al Qalah (Rohlich, 1974). The Formation is rich in fossils, where the most abundant taxa belongs to larger benthic foraminifers, especially the *Nummulites* which sometimes build up a nummulitic bank and their related environments as back bank (lagoonal) and fore bank according the lithological textures and the contained micro/macrofossils assemblages. Elwerfalli and Stow, (2008), grouped the Lower Tertiary deposits including the Darnah Formation into three main groups, i) the slope facies association; ii) the shallow marine facies association and iii) The lagoonal (back bank) facies association.

Darnah Formation at the basal part of Al Hamadah roadcut section is subjected to sampling herein. Darnah Formation at this roadcut section made up with about 80m thick, it consists of six units, (Fig.2.26) these are from base to top: i) Limestone interbedded with maly limestone containing chert nodules. ii) Thin bed of limestone enriched with *Ditruba* worm tubes. iii) Skeletal Limestone with common *Nummulites* and mollusk. iv) Nummulitic limestone locally dolomitized v) *Orbitolites* bed and vi) Nummulitic limestone with dominant *N. gizehensis*. For more detail information about this section Elwerfalli et al., (2000) is recommended.

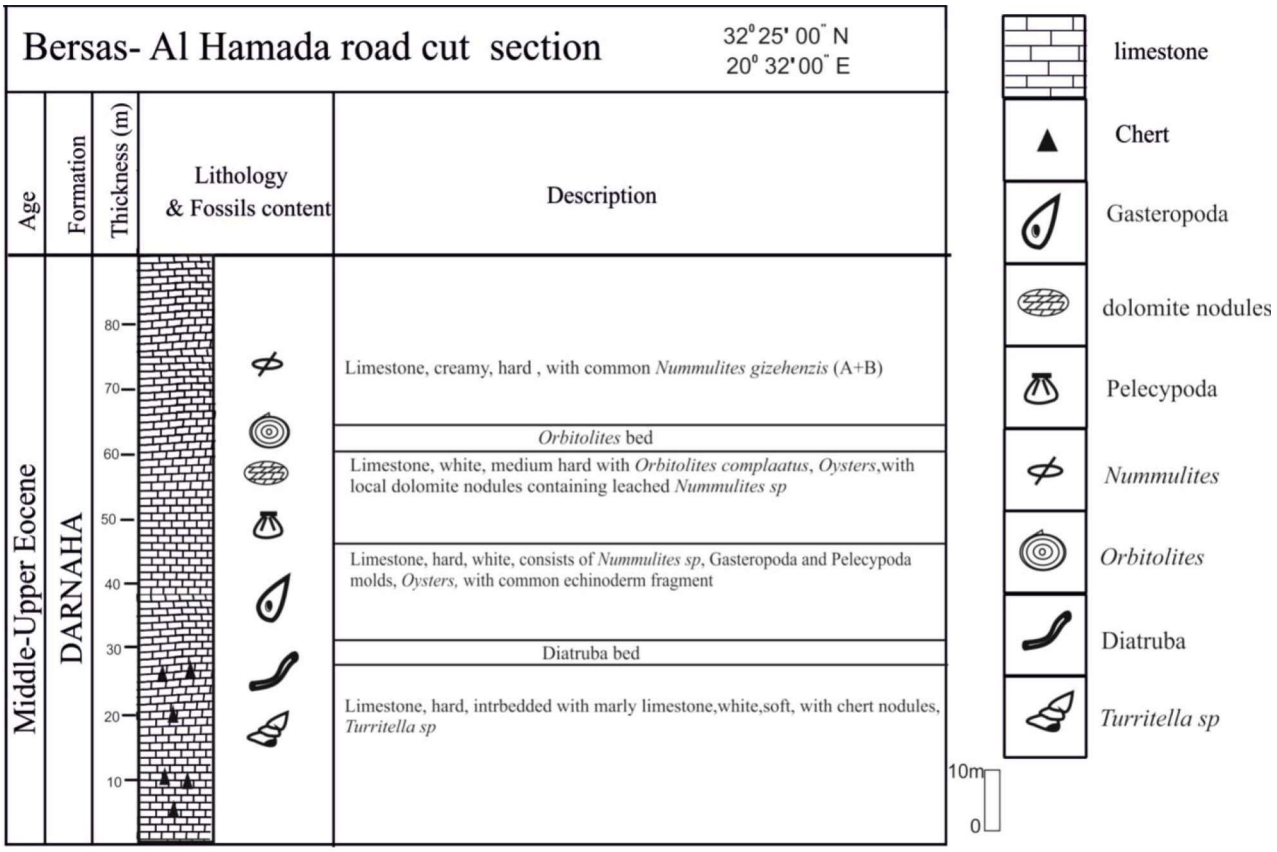

Fig. 2.26.**:** Lithological column of Darnah Formation at Bersas- Al Hamada road cut Al Jabal al Akhdar, Libya

The diagnostic *Nummulites gizehensis, Orbitolites complanata, Sphaerogypsina globula* and common molloscan shell concentrations are occurred throughout the section, with characteristic horizon of calcified worm tube "Diatruba". Chert nodules are also a common character at the lower unit (26m thick) which displays alternation of marly limestone, white, soft- medium hard, chalky and locally contained small sized *Nummulites* sp. and few echinoderm debris. This lower intervals yielding chert nodules (Figs. 2.27 a,b) and (Figs. 2.29) of brownish with concentric colored silica overgrowth and *Nummulites gizehensis* (Figs. 28) with euhedral floating dolomite crystals within chert matrix indicating replacement of calcite by chert , occur at a much more rapid rate than that of dolomite (Flugel,2010), (Fig 2.30).

Fig 2.27: a) General veiw of chert nodules in Darnah Formation; b) close up of the cherts and the host rock as well, (the base of Barsas-Al Hamda roadcut.

Fig. 2.28: Photomicrographs of (M) microcrystalline quartz matrix with silica (R) replaced the (N) *Nummulites* tests, from Darnah Formation at Barsas-Al Hamda roadcut. Sample no. (15)

Fig. 2.29: photomicrographs of chert-limestone contact from Darnah Formation at Barsas-Al Hamda roadcut.

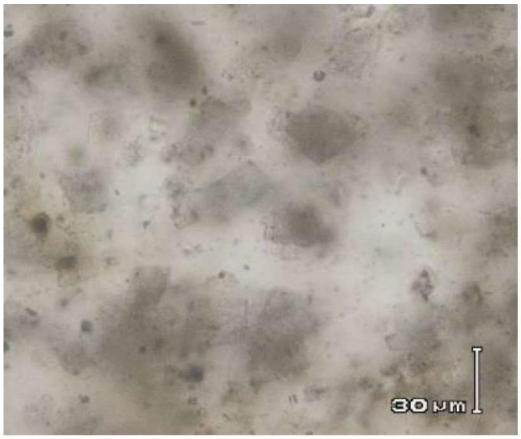

Fig. 2.30: Photomicrograph of chert of Darnah Formation shows floated dolomite crystals, from Barsas-Al Hamda roadcut section. Sample no. (17)

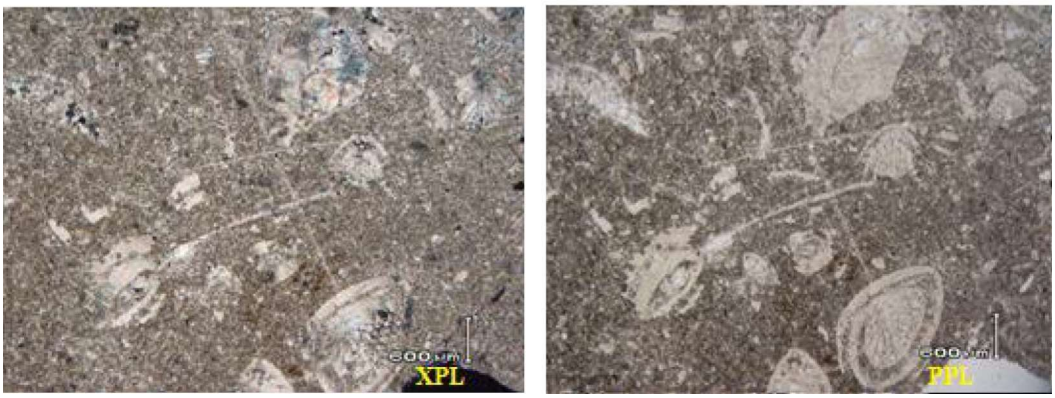

Fig. 2.31: Photomicrographs of wackestone with rich *Nummulites* and sponge spicules-like from Barsas-Al Hamda roadcut section. Sample no. (18)

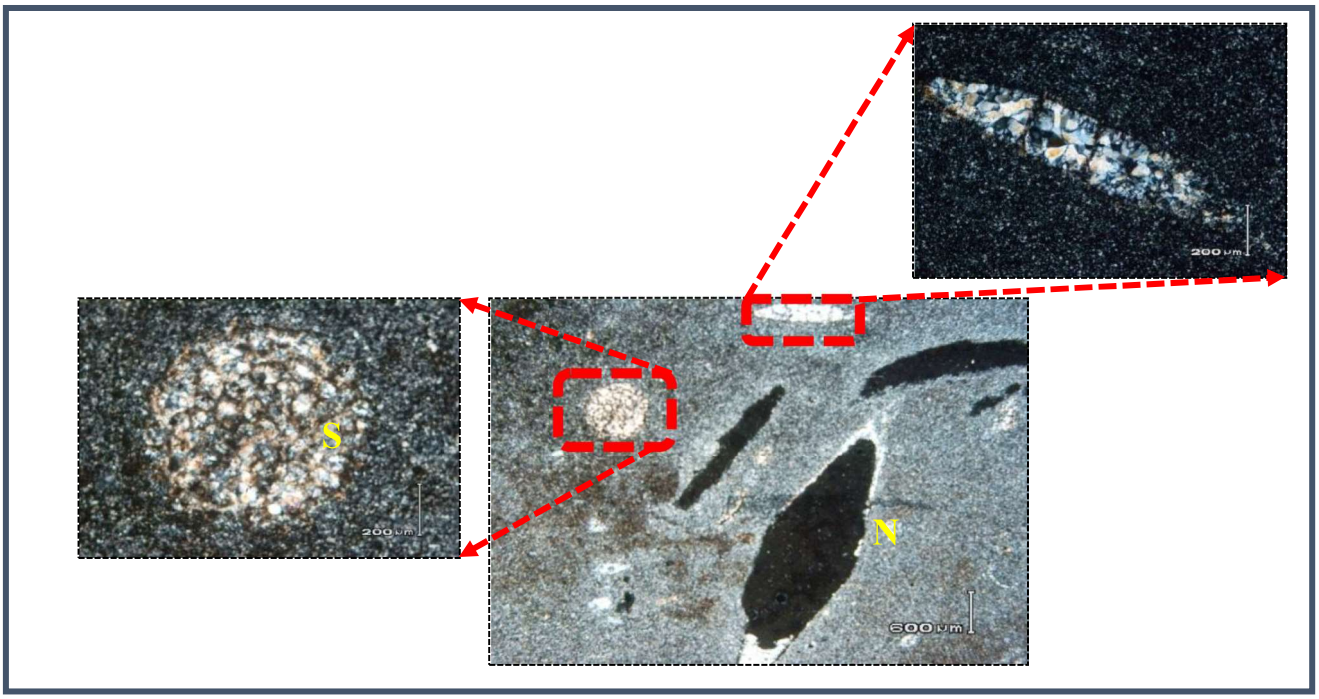

Fig. 2.32: Photomicrographs of leached (in black) and silicified *Nummulites* sp. (N), and *Sphaerogypsina globula* (S) from Darnah Formation at Barsas-Al Hamda roadcut section. Sample no. (20)

2.1.4 Wadi Al Qattarah Formation (Late Miocene)

It consists of 27m sequence at the type locality represents shallow water deposits with significant brackish condition. It composes of grayish white, soft, oolitic limestone, cross bedded with gypsum crystals and nodules of gray chert in the upper part, at the basal part it contains glauconitic marl, marly limestone, with local lenses and irregular bodies of gypsum, (Fig. 2.34).

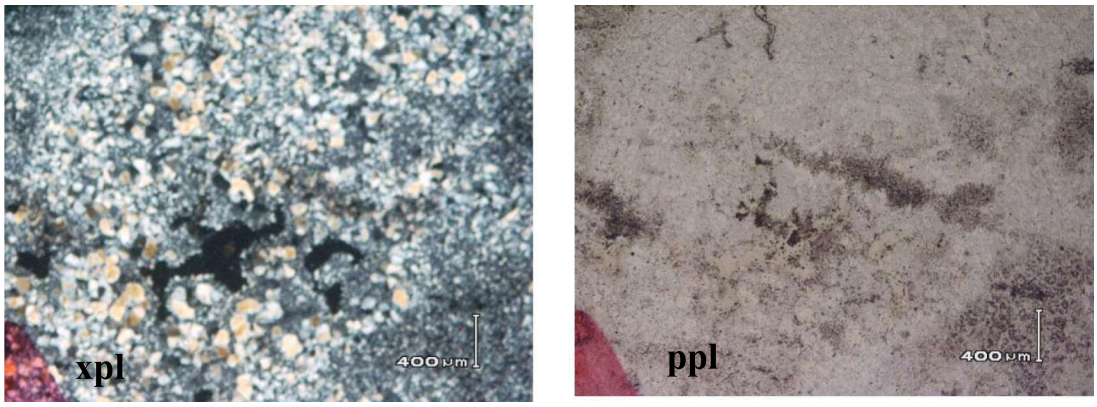

Fig. 2.33: photomicrograph of microcrystalline quartz wadi Qattarh FM, ppl ,xpl Sample19

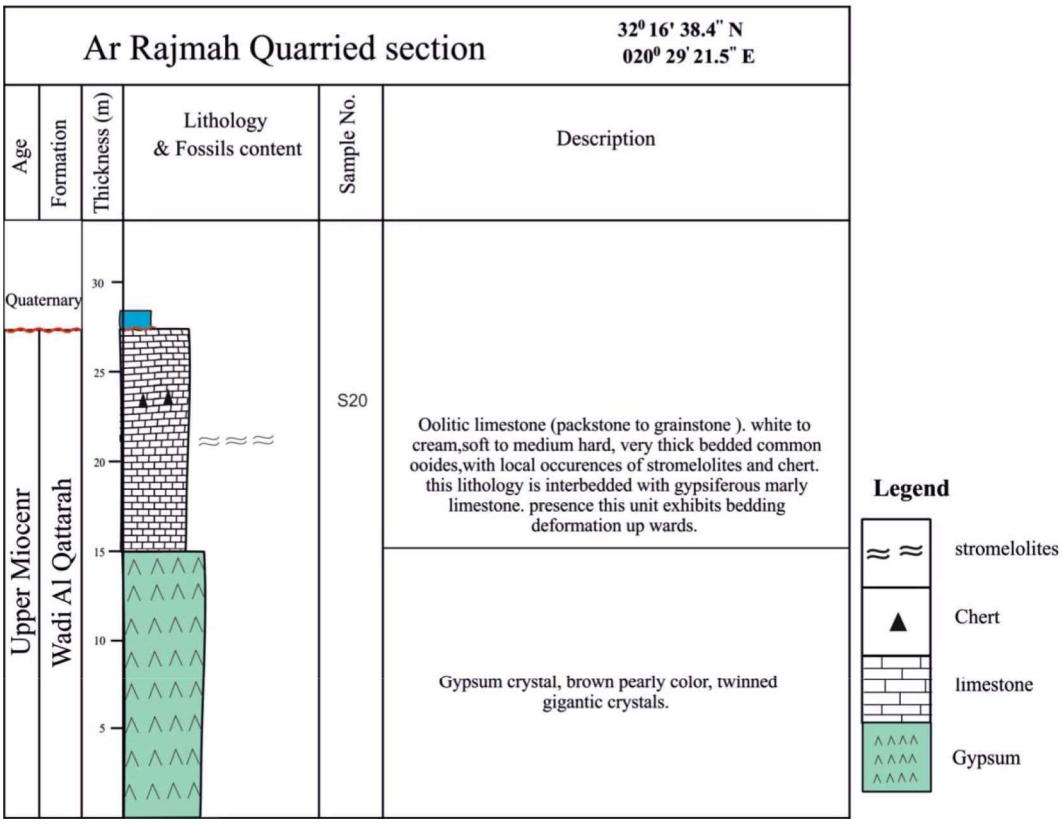

Fig. 2.34: Lithologic column of Wadi Al Qattarah Formation at Ar Rajmah Quarry

At the studied Quarry; Wadi al Qattarah composed of 15m gypsum depsits as the lower unit characterized by brownish green color with pearly appearance, very hard, massive gigantic crystals, twinned overlaind by oolitic limestone, packstone-grainstone texture, white to cream, soft-medium hard, thick-very thick beeded, with common ooids, of *stromatolites (*Fig 2.35 a), with localy occurrences rare moliolids.

Chert are sparsely as whitish gray, bluish gray, very hard, nodules with irregular periphery (Fig 2.35b)

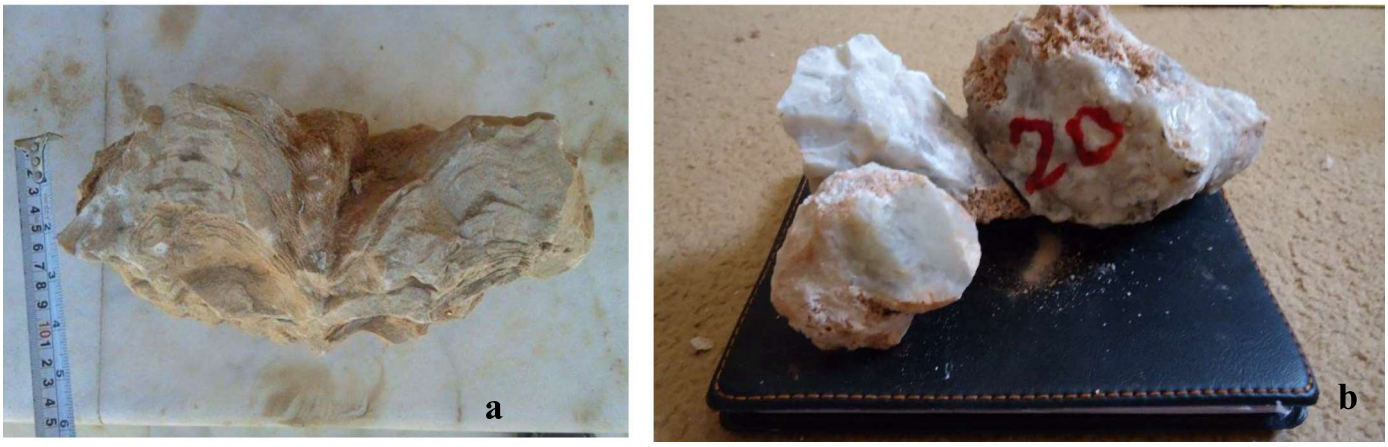

Fig 2.35: *Stromatolites, (*a), and chert (b) in Wadi Al Qattarah Formation at Ar Rajmah Quarry

CHAPTER THREE
GEOCHEMISTRY

3.1. Introduction

A chert is a chemically precipitated sedimentary rock, essentially monomineralic, and composed chiefly of microcrystalline and/or chalcedonic quartz, with subordinate megaquartz (Folk, 1980). Cherts may contain up to 95% or more SiO_2 (Hesse, 1988). The increase of SiO_2 concentration has two significant effects on the chemical characterization potential of depositional environments. First, SiO_2 acts as a dilutant, with final the SiO_2 concentration in chert often exceeding 95% (Murray, 1994). Cherts are chemically inert and markedly resistant to weathering and alteration, making them suitable for geochemical studies. Previous studies of cherts mainly focused on their origin or depositional environment and few studies examined the evolutionary processes of basins. Major oxides (especially TiO_2, Al_2O_3 and Fe_2O_3) and rare earth elements (REE) of cherts, because of their immobility during diagenesis (Murray *et al*., 1992), can reflect minor constituents such as hydrothermal precipitates, volcanic detritus, and terrigenous clasts, and hence are a key indicator to assess the depositional environment (Sugisaki *et al*., 1982; Yamamoto, 1987; Murray, 1994; Kato and Nakamura, 2003; Yu *et al*., 2009; Wen *et al.,* 2016).

The purpose of the present chapter is to investigate the origin, depositional environment, paleocondition, paleoweathering, paleoclimate and tectonic setting of the cherts at Al Jabal Al Akhdar, NE Libya. The concentrations of major oxides, TOC and trace elements are shown in tables (3.1-3).

3.2. Statistical treatment

The statistical treatment of the present data involves descriptive statistics, correlation matrix and factor analysis (Tables 3.4-6) using the SPSS© program. The descriptive statistics indicate that the studied cherts contain high concentrations of heavy metals (Ni, Co, V and Cr), high field strength elements (Zr, Hf, Nb, Ta, Th and U) and pseudolanthanides (Y and Sc), and low concentrations of TOC and rare earth elements.

Table 3.1: Chemical analysis data (major oxides and TOC in wt%, $\delta^{30}Si$ in ‰, trace elements in ppm) of the chert from Athrun Formation

Formation	Athrun				
Location	Mouth of Wadi Athrun				
Lithology	Chert				Limestone
Sample No.	1	2	3	4	5
SiO_2	83.70	65.30	43.00	68.71	10.20
$\delta^{30}Si$	3.95	2.55	1.94	2.00	0.66
TiO_2	0.23	0.38	0.38	0.39	0.03
Al_2O_3	6.28	8.00	8.65	10.75	3.51
Fe_2O_3	2.21	1.98	1.44	1.81	1.74
MnO	0.08	0.03	0.03	0.05	0.01
MgO	0.80	1.82	1.69	1.84	2.00
CaO	2.91	13.66	25.07	12.69	44.50
Na_2O	0.33	0.60	0.29	0.94	0.35
K_2O	1.00	4.43	4.70	3.00	0.16
SO_3	0.94	1.92	0.80	0.95	0.18
Cl	0.16	0.33	0.20	0.55	0.20
P_2O_5	0.05	0.08	0.07	0.09	0.11
TOC	0.44	0.62	0.55	0.81	0.26
Ge	0.65	0.51	0.28	0.35	0.48
Ni	319.7	265.86	257.21	266	211.67
Co	516	462.2	453.55	462.34	408
V	1052.8	844.66	819.92	825	772.4
Cr	1039.67	831.53	806.79	811.87	759.27
Zr	217.45	133.31	100.23	119.19	77.20
Hf	2.90	1.76	0.68	1.64	0.65
Nb	162.26	78.17	45.24	64.36	23.44
Ta	1.50	1.00	0.28	0.93	0.35
Sc	215.00	130.91	98.14	117.10	75.11
Th	216.93	132.84	99.91	119.03	78.11
U	15.25	17.29	14.36	13.48	12.56
Y	171.36	117.52	108.87	117.66	63.33
La	0.69	0.67	0.71	0.65	0.69
Ce	0.19	0.21	0.22	0.17	0.13
Pr	0.68	0.69	0.70	0.64	0.65
Nd	0.73	0.75	0.71	0.70	0.75
Sm	0.80	0.81	0.78	0.78	0.81
Eu	0.85	0.87	0.89	0.78	0.83
Gd	0.79	0.80	0.82	0.79	0.80
Tb	1.14	1.11	1.19	1.10	1.15
Dy	1.17	1.15	1.14	1.15	1.17
Ho	1.22	1.20	1.25	1.19	1.19
Er	1.24	1.26	1.30	1.23	1.22
Tm	1.19	1.21	1.23	1.18	1.18
Yb	1.15	1.14	1.17	1.13	1.10
Lu	1.07	1.00	1.05	1.05	1.04

Table 3.2: Chemical analysis data (major oxides and TOC in wt%, $\delta^{30}Si$ in ‰, trace elements in ppm) of the chert from Apollonia Formation

Formation	Apollonia									
Location	Pyramid section (Wadi Karsa)					Wadi Athrun			Tuckra	
Lithology	Limestone		Chert		Limestone	Chert	Limestone		Chert	Limestone
Sample No.	6	7	8	9A	9B	10	11	12	13	14
SiO_2	7.50	6.25	73.61	80.55	6.83	89.41	11.90	8.00	67.21	4.48
$\delta^{30}Si$	0.81	0.67	3.00	3.98	0.93	3.67	0.56	0.59	1.46	0.61
TiO_2	0.04	0.06	0.28	0.33	0.03	0.18	0.04	0.02	0.47	0.02
Al_2O_3	2.48	1.95	9.90	6.26	1.86	3.27	1.57	2.90	11.18	0.77
Fe_2O_3	1.33	1.19	3.78	3.85	0.95	1.50	0.73	1.14	2.51	0.49
MnO	0.02	0.02	0.05	0.03	0.01	0.04	0.02	0.01	0.08	0.02
MgO	2.13	0.48	0.83	0.47	0.69	0.45	0.91	1.22	1.28	1.12
CaO	45.90	50.55	3.71	0.14	48.58	0.33	45.91	46.69	5.85	51.91
Na_2O	0.19	0.23	0.31	0.49	0.13	0.24	0.29	0.42	0.48	0.65
K_2O	0.12	0.39	1.56	1.36	0.10	0.77	0.19	0.29	2.70	0.13
SO_3	0.09	0.08	0.19	0.11	0.08	0.07	0.08	0.11	0.07	0.09
Cl	0.15	0.09	0.14	0.09	0.07	0.09	0.17	0.31	0.12	0.44
P_2O_5	0.13	0.13	0.07	0.09	0.09	0.06	0.09	0.05	0.09	0.05
TOC	0.31	0.29	0.79	0.40	0.27	0.37	0.23	0.33	0.87	0.21
Ge	0.44	0.51	0.39	0.59	0.47	0.49	0.42	0.33	0.39	0.29
Ni	204.5	228.1	289.7	350.4	215.62	321.16	205	208.2	263.36	221.05
Co	400.8	424.5	486.1	546.7	411.96	517.5	401.3	404.5	459.7	417.39
V	765.5	791	944.5	1067	786.52	1098.77	800.1	769.7	900.18	775.09
Cr	752.3	777.9	931.4	1054	773.39	1085.64	787	756.6	887.05	761.96
Zr	70.75	89.10	171.30	222.21	60.00	245.07	71.72	80.55	122.54	77.05
Hf	1.20	0.55	2.75	2.66	0.45	1.52	1.17	1.11	1.99	0.50
Nb	15.88	34.33	116.47	167.78	5.17	190.24	17.00	25.72	67.71	22.22
Ta	0.61	0.25	1.35	1.26	0.25	1.12	0.57	0.66	0.98	0.29
Sc	68.66	87.11	169.21	220.12	57.91	242.98	69.63	78.46	120.45	74.96
Th	70.59	89.00	171.14	222.45	59.84	244.91	71.56	80.39	122.38	76.89
U	5	3.45	25.59	26.9	4.29	29.36	6.11	4.84	16.83	11.34
Y	56.15	79.79	141.35	202.06	67.28	172.82	56.66	59.83	115.02	72.71
La	1.00	1.05	0.88	0.86	1.05	0.83	1.10	1.11	0.80	1.09
Ce	0.13	0.15	0.18	0.22	0.13	0.17	0.16	0.14	0.15	0.17
Pr	0.72	0.70	0.67	0.65	0.69	0.67	0.68	0.73	0.69	0.71
Nd	0.76	0.76	0.72	0.70	0.78	0.73	0.80	0.79	0.73	0.77
Sm	0.80	0.78	0.79	0.85	0.81	0.81	0.79	0.80	0.84	0.80
Eu	0.85	0.87	0.82	0.88	0.89	0.84	0.85	0.82	0.86	0.83
Gd	0.78	0.76	0.78	0.81	0.76	0.79	0.81	0.80	0.77	0.79
Tb	1.05	1.09	1.17	1.16	1.05	1.19	1.07	1.09	1.19	1.10
Dy	1.09	1.05	1.20	1.20	0.94	1.19	1.00	0.97	1.22	0.98
Ho	1.16	1.13	1.25	1.26	1.19	1.23	1.18	1.16	1.27	1.12
Er	1.19	1.21	1.29	1.31	1.22	1.33	1.22	1.18	1.25	1.16
Tm	1.14	1.10	1.25	1.29	1.13	1.25	1.11	1.11	1.28	1.12
Yb	1.10	1.08	1.18	1.11	1.06	1.19	1.09	1.10	1.16	1.11
Lu	1.08	1.11	1.05	1.09	1.09	1.04	1.11	1.12	1.10	1.13

Table 3.3: Chemical analysis data (major oxides and TOC in wt%, $\delta^{30}Si$ in ‰, trace elements in ppm) of the chert from Darnah and Wadi Al Qattarah formations

Formation	Darnah						Wadi Al Qattarah
Location	Al Hamada						Daryanah-Abyar
Lithology	Chert	Limestone	Chert				Chert
Sample No.	15	16	17	18	19A	19B	20
SiO_2	78.68	5.57	72.65	65.21	80.66	74.82	76.35
$\delta^{30}Si$	3.70	0.90	2.68	1.73	3.88	3.08	3.31
TiO_2	0.45	0.03	0.30	0.50	0.32	0.36	0.32
Al_2O_3	6.44	1.92	5.28	10.12	5.71	8.87	8.09
Fe_2O_3	3.69	0.78	2.91	2.68	2.79	4.10	2.23
MnO	0.06	0.02	0.05	0.08	0.09	0.06	0.07
MgO	0.54	1.00	1.08	1.77	1.10	0.79	0.76
CaO	0.18	50.08	6.55	7.80	1.05	0.46	2.49
Na_2O	0.72	0.41	0.37	0.67	0.52	0.72	0.57
K_2O	1.75	0.22	1.26	4.23	1.57	2.73	2.32
SO_3	0.12	0.10	0.45	0.07	0.09	0.09	0.08
Cl	0.37	0.23	0.18	0.30	0.32	0.31	0.23
P_2O_5	0.12	0.06	0.21	0.09	0.07	0.09	0.12
TOC	0.43	0.29	0.39	0.80	0.40	0.69	0.68
Ge	0.51	0.42	0.58	0.49	0.52	0.53	0.44
Ni	280.24	225.19	285.31	265.3	325	284.12	275.42
Co	476.58	421.53	481.65	461.64	521.34	471.76	480.46
V	972.23	793.63	977.81	845.45	1075.25	950.76	989.40
Cr	959.1	780.5	964.68	832.32	1062.12	937.63	976.27
Zr	188.21	59.11	165.65	82.00	232.11	190.87	171.91
Hf	1.66	0.56	1.10	1.45	1.56	2.32	2.36
Nb	133.58	4.26	110.82	27.17	177.26	136.09	117.21
Ta	1.26	0.26	0.70	0.70	1.16	1.52	1.26
Sc	186.12	57.00	163.56	79.91	230.00	188.78	169.82
Th	188.25	58.93	165.49	81.84	231.93	190.71	171.75
U	32.7	3.38	29.94	16.29	26.38	35.16	26.33
Y	131.90	76.85	136.97	116.96	176.66	135.78	127.08
La	0.10	0.16	0.13	0.14	0.16	0.09	0.10
Ce	0.07	0.09	0.06	0.06	0.08	0.05	0.07
Pr	0.13	0.17	0.15	0.16	0.14	0.10	0.12
Nd	0.23	0.20	0.25	0.25	0.27	0.21	0.16
Sm	0.29	0.24	0.31	0.33	0.33	0.29	0.20
Eu	0.31	0.27	0.30	0.32	0.31	0.29	0.26
Gd	0.34	0.31	0.34	0.36	0.37	0.33	0.32
Tb	0.39	0.33	0.42	0.42	0.44	0.39	0.36
Dy	0.44	0.39	0.46	0.48	0.48	0.42	0.43
Ho	0.48	0.43	0.49	0.51	0.52	0.48	0.48
Er	0.50	0.45	0.50	0.53	0.54	0.48	0.50
Tm	0.51	0.45	0.53	0.55	0.57	0.50	0.49
Yb	0.43	0.38	0.45	0.44	0.44	0.42	0.40
Lu	0.46	0.41	0.48	0.48	0.50	0.44	0.45

Table 3.4: Descriptive statistics of the studied samples (major oxides and TOC in wt%, trace elements in ppm)

Oxides and elements	N	Min	Max	Mean	Std. Deviation
SiO_2	22	4.48	89.41	49.12	33.34
TiO_2	22	0.02	0.50	0.23	0.17
Al_2O_3	22	0.77	11.18	5.72	3.36
Fe_2O_3	22	0.49	4.10	2.08	1.09
MnO	22	0.01	0.09	0.04	0.03
MgO	22	0.45	2.13	1.13	0.53
CaO	22	0.14	51.91	21.23	21.52
Na_2O	22	0.13	0.94	0.45	0.21
K_2O	22	0.10	4.70	1.59	1.49
SO_3	22	0.07	1.92	0.31	0.46
Cl	22	0.07	0.55	0.23	0.12
P_2O_5	22	0.05	0.21	0.09	0.04
TOC	22	0.21	0.87	0.47	0.21
Ge	22	0.28	0.65	0.46	0.10
Ni	22	204.49	350.40	262.19	43.26
Co	22	400.83	546.74	458.53	43.26
V	22	765.45	1098.77	891.71	114.40
Cr	22	752.32	1085.64	878.58	114.40
Zr	22	59.11	245.07	133.98	62.19
Hf	22	0.45	2.90	1.48	0.77
Nb	22	4.26	190.24	79.20	62.16
Ta	22	0.25	1.52	0.83	0.44
Sc	22	57.00	242.98	131.86	62.16
Th	22	58.93	244.91	133.86	62.16
U	22	3.38	35.16	17.13	10.37
Y	22	56.15	202.06	113.85	43.26
REE	22	4.30	13.39	10.34	3.96

Table 3.5: Correlation matrix of the studied samples

	SiO_2	TiO_2	Al_2O_3	Fe_2O_3	MnO	MgO	CaO	Na_2O	K_2O	SO_3	Cl	P_2O_5	TOC	Ge	Ni	Co	V	Cr	Zr	Hf	Nb	Ta	Sc	Th	U	Y	REE
SiO_2	1.00																										
TiO_2	0.82	1.00																									
Al_2O_3	0.72	0.90	1.00																								
Fe_2O_3	0.77	0.71	0.66	1.00																							
MnO	0.79	0.76	0.69	0.61	1.00																						
MgO	-0.24	0.07	0.22	-0.23	-0.10	1.00																					
CaO	-0.99	-0.84	-0.75	-0.82	-0.81	0.23	1.00																				
Na_2O	0.41	0.59	0.54	0.38	0.43	0.17	-0.42	1.00																			
K_2O	0.54	0.85	0.83	0.39	0.48	0.35	-0.56	0.50	1.00																		
SO_3	0.24	0.31	0.34	-0.02	0.03	0.40	-0.19	0.22	0.54	1.00																	
Cl	0.08	0.26	0.24	0.02	0.17	0.37	-0.07	0.85	0.32	0.30	1.00																
P_2O_5	0.05	0.12	0.01	0.24	0.03	0.05	-0.08	-0.07	-0.03	-0.09	-0.17	1.00															
TOC	0.62	0.81	0.96	0.54	0.65	0.21	-0.65	0.52	0.78	0.27	0.24	-0.03	1.00														
Ge	0.45	0.18	0.01	0.49	0.34	-0.35	-0.45	-0.09	-0.08	0.09	-0.34	0.34	-0.09	1.00													
Ni	0.91	0.64	0.50	0.71	0.66	-0.40	-0.89	0.25	0.34	0.15	-0.07	-0.06	0.37	0.55	1.00												
Co	0.91	0.63	0.50	0.69	0.66	-0.40	-0.89	0.24	0.34	0.15	-0.07	-0.05	0.37	0.54	0.99	1.00											
V	0.87	0.49	0.33	0.65	0.66	-0.54	-0.85	0.11	0.13	-0.03	-0.18	0.01	0.22	0.60	0.94	0.94	1.00										
Cr	0.87	0.49	0.33	0.65	0.66	-0.54	-0.85	0.11	0.13	-0.03	-0.18	0.01	0.22	0.60	0.94	0.94	0.99	1.00									
Zr	0.87	0.50	0.36	0.68	0.61	-0.49	-0.85	0.18	0.17	0.08	-0.07	-0.02	0.24	0.56	0.93	0.93	0.97	0.97	1.00								
Hf	0.78	0.57	0.63	0.73	0.63	-0.26	-0.80	0.29	0.31	0.17	-0.05	-0.12	0.59	0.42	0.73	0.73	0.70	0.70	0.72	1.00							
Nb	0.87	0.49	0.36	0.68	0.61	-0.49	-0.85	0.18	0.17	0.07	-0.07	-0.02	0.24	0.56	0.93	0.93	0.97	0.97	0.98	0.72	1.00						
Ta	0.86	0.59	0.58	0.77	0.69	-0.32	-0.87	0.38	0.29	0.13	0.08	-0.09	0.52	0.47	0.78	0.77	0.80	0.80	0.85	0.94	0.85	1.00					
Sc	0.87	0.50	0.36	0.68	0.61	-0.49	-0.85	0.18	0.17	0.07	-0.07	-0.02	0.24	0.56	0.93	0.93	0.97	0.97	0.98	0.72	0.98	0.85	1.00				
Th	0.87	0.49	0.36	0.68	0.61	-0.49	-0.85	0.18	0.17	0.07	-0.07	-0.02	0.24	0.56	0.93	0.93	0.97	0.97	0.99	0.72	0.98	0.85	0.98	1.00			
U	0.86	0.66	0.51	0.83	0.60	-0.34	-0.88	0.39	0.36	-0.01	0.09	0.22	0.41	0.41	0.79	0.78	0.81	0.81	0.84	0.61	0.84	0.77	0.84	0.84	1.00		
Y	0.91	0.64	0.50	0.71	0.66	-0.40	-0.89	0.25	0.34	0.15	-0.07	-0.06	0.37	0.55	1.00	1.00	0.94	0.94	0.93	0.73	0.93	0.78	0.93	0.93	0.79	1.00	
REE	-0.30	-0.34	-0.17	-0.39	-0.49	0.15	0.34	-0.41	-0.18	0.24	-0.29	-0.33	-0.16	-0.28	-0.21	-0.21	-0.28	-0.28	-0.21	-0.07	-0.21	-0.22	-0.21	-0.21	-0.46	-0.21	1.00

Table 3.6: Factor analysis of the studied samples

Eigenvalue	15.43	4.39	1.81	1.46
% of Variance	57.14	16.26	6.70	5.42
Cumulative %	57.14	73.40	80.09	85.51
Factor	1	2	3	4
SiO_2	0.98	0.14	0.04	0.05
TiO_2	0.75	0.58	-0.08	0.17
Al_2O_3	0.63	0.69	0.08	0.23
Fe_2O_3	0.82	0.12	-0.26	0.17
MnO	0.78	0.27	-0.18	0.00
MgO	-0.36	0.66	0.11	0.17
CaO	-0.98	-0.16	0.02	-0.08
Na_2O	0.37	0.66	-0.24	-0.51
K_2O	0.43	0.78	0.12	0.20
SO_3	0.14	0.45	0.50	0.12
Cl	0.03	0.64	-0.15	-0.68
P_2O_5	0.03	-0.05	-0.66	0.55
TOC	0.53	0.72	0.08	0.21
Ge	0.53	-0.43	-0.20	0.30
Ni	0.95	-0.14	0.13	-0.02
Co	0.95	-0.14	0.13	-0.01
V	0.92	-0.35	0.01	-0.04
Cr	0.92	-0.35	0.01	-0.04
Zr	0.93	-0.29	0.08	-0.11
Hf	0.82	0.06	0.22	0.07
Nb	0.93	-0.29	0.08	-0.11
Ta	0.90	0.01	0.08	-0.09
Sc	0.93	-0.29	0.08	-0.11
Th	0.93	-0.29	0.08	-0.11
U	0.88	-0.01	-0.26	-0.05
Y	0.95	-0.14	0.13	-0.02
REE	-0.33	-0.13	0.81	0.17

The factor analysis is a powerful tool for identifying relationships that are not readily evident from simple correlation analysis. The extracted varimax R-mode factor matrix is represented in table 3.6. Four factors explaining approximately 85.51% of the total variables are extracted. The variances of each factor reflect the amount of the total data contained in it. These

four factors summarize the main geochemical controls affecting the abundance and distribution of the analyzed major oxides, TOC and trace elements in the studied samples.

Factor one (F1): It is the strongest factor as it accounts for about 57.14% of the variables. It shows positive loading for SiO_2, TiO_2, Al_2O_3, Fe_2O_3, MnO, TOC, heavy metals (Ge, Ni, Co, V and Cr), high field strength elements (Zr, Hf, Nb, Ta, Th and U) and pseudolanthanides (Y and Sc). This factor displays negative loading for CaO. This factor seems to be significant in interpreting the origin of silica.

Factor two (F2): It accounts for 16.26% of the total variables, where it shows positive loading for TiO_2, Al_2O_3, MgO, Na_2O, K_2O, Cl and TOC. Therefore, this factor represents the prominent influence of the clayey material on the geochemistry of the studied samples.

Factor three (F3): It accounts for 6.70% of the total variables. It shows positive loading for SO_3 and REE, while it displays negative loading for P_2O_5.

Factor four (F4): It is the weakest where it represents only 5.42% of the total variables especially P_2O_5.

The statistical treatment suggests that the analyzed major oxides, TOC and trace elements are possibly of marine source. However, continental contamination (terrigenous influx) has drastically altered the biochemical and geochemical cycles and the balance of some elements.

3.3. Normalization to Post Archean Australian Shale (PAAS)

The average chemical composition of the studied samples are normalized using PAAS values (Taylor and McLennan 1985) and are given in the histogram diagram (Fig. 3.1) which shows the variations of individual elements against the standard shale (PAAS). Fig (3.1) shows that:

1) There are notable depletions in most major oxides (except SiO_2 and CaO).
2) There are obvious enrichments in most trace elements (except Zr, Hf and REE).

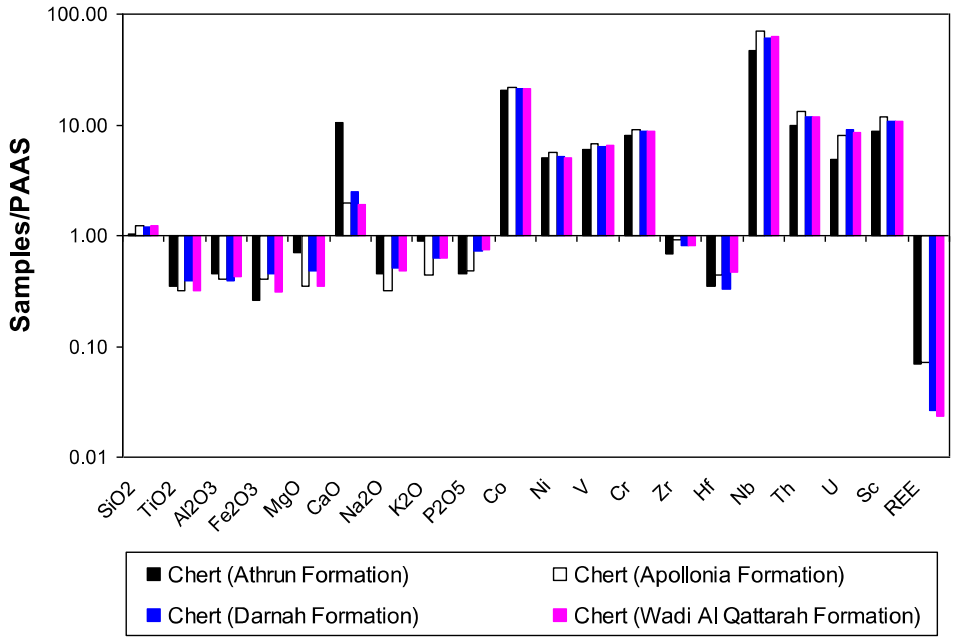

Fig. 3.1: Major oxides and trace elements content of the studied samples normalized to the PAAS (Taylor and McLennan, 1985)

3.4. Major oxides

3.4.1. Silica (SiO_2)

In the present study, the SiO_2 content ranges from 4.48 to 11.9% for the limestone samples, and 43 to 89.41% for the chert samples. In general the high concentration of SiO_2 in limestones indicate the influence of terrigenous influx during deposition and low concentration of SiO_2 reflect restricted supply of terrigenous clastic sediment with respect to the basin. The correlation matrix shows that SiO_2 is positively correlated with TiO_2, Al_2O_3, Fe_2O_3, MnO and TOC (r = 0.82, 0.72, 0.77, 0.79 and 0.62, respectively). The SiO_2 concentration exhibits high degree of inverse correlation with CaO (r = -0.99), which indicates the gradual decrease in calcite and subsequent enrichment of silicates (free silica and aluminosilicates). The SiO_2/Al_2O_3, as a relative measure of free to combined silica, decreases from 27.34 (i.e., maximum free and least combined silica) for the chert samples to 2.76 for the limestone samples.

3.4.2. Alumina (Al_2O_3) and relevant oxides

Aluminum is not normally substituted in carbonate mineral. The measure of Al is directly linked with the influx of detrital sediments to the depositional site (Botz *et al.,* 1988). Buckley and Cranston (1991) inferred that the variations of Al_2O_3 in sediments might be associated with changes in clay mineral content or with the content of feldspars in the sediment. The detrital clastic source can be revealed by the relations between concentration of Al_2O_3, an abundance of lithogenic element, and concentrations of other elements. If I assume that Al_2O_3 is derived from detrital aluminosilicate sources, then essentially all of the Fe_2O_3 and TiO_2 appear to be contributed by lithogenic detritus. The correlation matrix shows that Al_2O_3 is positively correlated with SiO_2, TiO_2, Fe_2O_3, MnO, K_2O and TOC (r = 0.72, 0.90, 0.66, 0.69, 0.83 and 0.96, respectively).

Potassium is not suitable as a paleosalinity indicator like sodium (Veizer, 1978). K concentrations are dependent of the primary chemical composition of the interstitial water and secondary enrichment during diagenesis through neomorphism of carbonate (Morton, 1985). The carbonate minerals themselves contain small amount of potassium. K content is less affected by the diagenesis of carbonate minerals; it decreases with increasing time of diagenesis. Also, the K content of carbonate rocks does not decrease as much with time as Na (Molenaar and Jong, 1987). During replacement of aragonite by calcite, small amounts of K are expected to be liberated into the interstitial water (White, 1977a). The positive correlation between K_2O and Al_2O_3 in the studied samples suggesting, that they are bound to alumino-silicate minerals. According to Cox *et al.,* (1995) the K_2O/Al_2O_3 ratios for clay minerals and feldspars are different (0.0 to 0.3, 0.3 to 0.9, respectively). In the present study, the K_2O/Al_2O_3 ratio ranges 0.05 to 0.3, indicating that clay minerals have a major role in the distribution of aluminum in the studied samples. The presence of clay minerals in the studied cherts is also supported by positive correlation between Al_2O_3 and $K_2O + Na_2O$ (Fig. 3.2). This scenario is also supported by higher K_2O/Na_2O in the cherts because K is more strongly than Na to be incorporated into clay minerals and Na is more prone to coprecipitate with carbonate (Fig. 3.3).

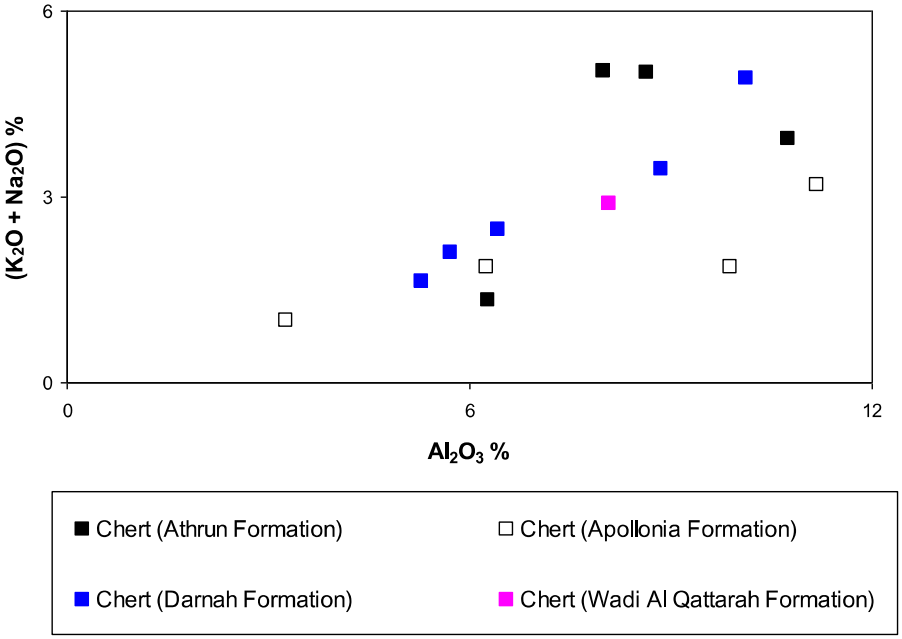

Fig. 3.2: Relationship between Al_2O_3 and (K_2O + Na_2O) in the studied chert samples

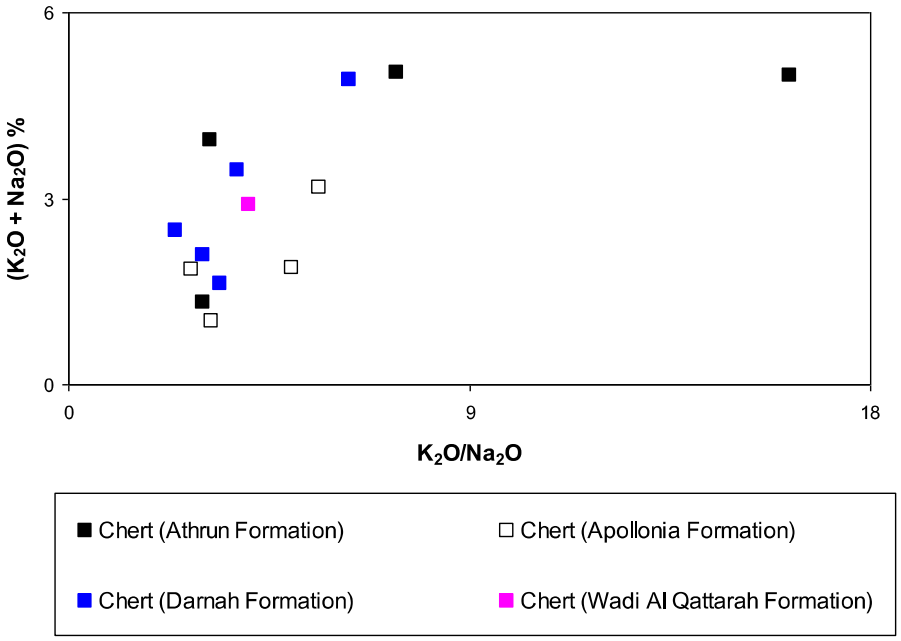

Fig. 3.3: Relationship between K_2O/Na_2O and (K_2O + Na_2O) in the studied chert samples

According to Brand (1989) the presence of iron in carbonate rocks can be explained by two factors:

1) The iron incorporated within calcite during precipitation of calcite in reducing condition of diagenetic environments.

2) The result of input and sedimentation rate of detrital material into the depositional environment.

Minor amount of Fe^{2+} (several thousand ppms) may also substitute for Ca^{2+} in calcite or for Mg^{2+} in magnesian calcite giving ferroan calcite (Fe-calcite). In the present study, the Fe_2O_3 content ranges from 0.49 to 1.74% for the limestone samples, and 1.44 to 4.1% for the chert samples. The low content indicates the depletion of pore fluid iron content during precipitation of calcite due to decrease in supply of detrital materials (Brand, 1989).

3.4.3. Soda (Na_2O)

Sodium, the most abundant cation in seawater, should be a good indicator of salinity during marine carbonate precipitation if it is partitioned into $(Ca,Mg)CO_3$ lattices in some consistent manner, and if lattice-bound sodium can be distinguished from trapped and adsorbed sodium (Veizer *et al.,* 1977). In general, Na content decreases drastically with time and increasing degree of carbonate diagenesis. The ancient carbonates have been most affected by such diagenetic processes; and even the recent carbonates have also been subjected to changes in the sodium content due to diagenetic alteration such as replacement, neomorphism etc (Veizer *et al.,* 1977). White (1977a) showed experimentally that Na co-precipitation in carbonate structures is independent of Mg concentration, suggesting that coexisting calcite and dolomite should have similar carbonate minerals, and that its bulk content in a carbonate rock will depend on the proportion of calcite and dolomite. The studied samples contain low concentrations of Na_2O (from 0.37 to 0.66). The author believes that the low Na_2O content in the samples may be due to intermittent influx of fresh water into the basin of deposition and prolonged diagenesis in an environment less saline than normal seawater.

3.4.4. Lime (CaO) and Magnesia (MgO)

Magnesium, originally deposited within the skeletons of living organisms, commonly remains within the rocks throughout the process of lithification and uplift. In carbonates rocks gaining of some amount of Mg are by removal of magnesium from the rock by moving waters (Chave, 1962). The Mg values can vary by the diagenetic equilibration of $CaCO_3$ with meteoric water depends on mineralogy and other factors causing either addition or depletion of magnesium (Brand and Veizer, 1980). In the present study, CaO and MgO do not demonstrate any confident coherence to any of the analyzed major oxides. Moreover, CaO is weakly correlated with MgO (r = 0.23, Fig. 3.4). The studied samples show low concentrations of MgO. The Mg values are very low, indicating the prevalent less saline and/or freshwater diagenesis by which extensive leaching can take place and is possible during later stages of diagenesis (Wilkinson and Given, 1986).

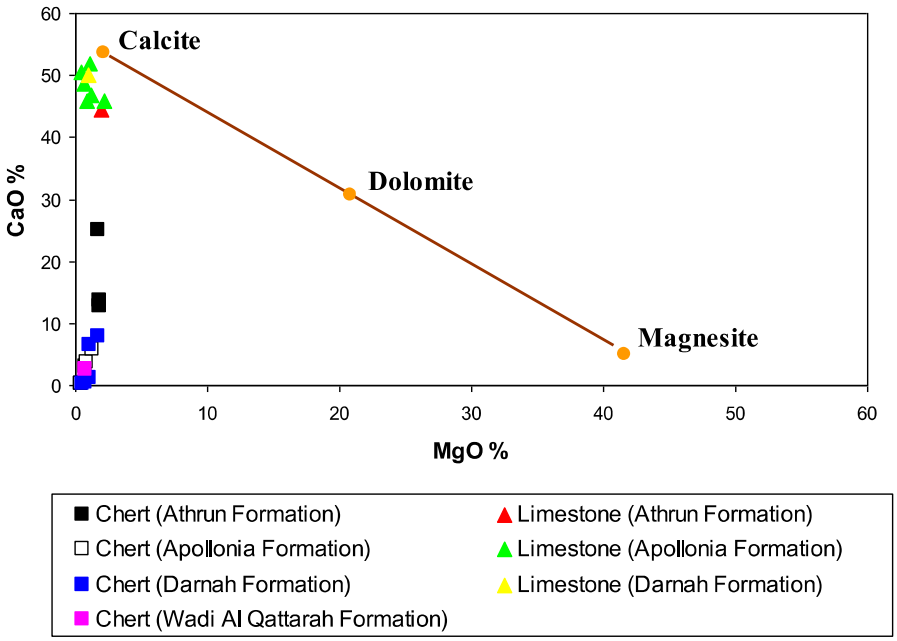

Fig. 3.4: Relationship between magnesia and lime in the studied samples (fields after Udayanapillai and Ganesa Moorthi, 2014)

It should be noted that the studied samples contain low concentrations of other major oxides (MnO, SO_3, Cl and P_2O_5).

3.5. Total Organic Carbon (TOC)

Organic carbon in the form of kerogen is the remnant of ancient life preserved in sedimentary rocks, after degradation by bacterial and chemical processes, and further modified by temperature, pressure, and time. The latter step, called thermal maturation, is a function of burial history (depth) and proximity to heat sources. Maturation provides the chemical reactions needed to give us gas, oil, bitumen, pyrobitumen, and graphite (pure carbon) that we find while drilling wells for petroleum. Organic carbon is usually associated with shales or silty shales, but may be present in relatively clean siltstone, sandstone and carbonate rocks. According to the classification given by Peters and Cassa (1994, Table 3.7), the studied samples can be rated as having a fair hydrocarbon potential (0.53 to 0.75%).

Table 3.7: Classification of TOC (after Peters and Cassa, 1994)

Petroleum Potential	TOC (wt. %)
Poor	0–0.5
Fair	0.5–1
Good	1–2
Very Good	2–4
Excellent	>4

According to Bouchez *et al.,* (2011) high Al/Si indicates Al-rich fine-grained sediment, whereas low Al/Si suggests Si-rich particles of larger grain size. Fig (3.5) shows that the data of the studied cherts fall in the field of grains, indicating that grains carry more TOC than mud.

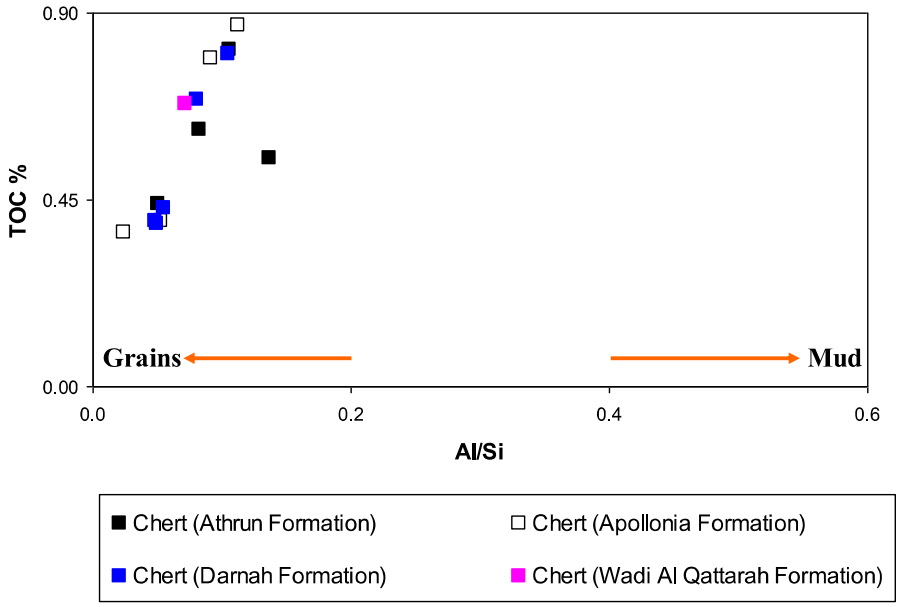

Fig. 3.5: Relationship between Al/Si and TOC in the studied cherts (modified after Sun et al., 2016)

3.6. Trace elements

In the present study, the analyzed trace elements include heavy metals such as Ge, Ni, Co, V and Cr, high field strength elements (HFSE) such as Zr, Hf, Nb, Ta, Th and U and rare earth elements (REE) such as La, Ce, Pr, Nd, Sm, Eu, Gd, Tb, Dy, Ho, Er, Tm, Yb and Lu, and related elements (Y and Sc).

3.7. Origin of chert

Extensive studies of marine sediments and sedimentary rocks have demonstrated that cherts in recent and ancient oceanic deposits are altered by fractionation and migration of some chemical elements during diagenesis (e.g., Ran *et al.,* 2015). These elements include biogenic SiO_2, K, Na, Ge, Co and B. They have tendencies to migrate into beds enriched in silica, whereas some elements such as Mn, Ca, Mg, P, Sr, V and Ba are remobilized and removed (Murray, 1994). The migration of Mn is further enhanced during subduction–accretion processes involving pelagic sediments. According to Rangin *et al.,* (1981) the Si/(Si+Fe+Al+Ca) ratio can be presented information on the content of biogenic silica with respect to aluminosilicates and ferruginous and calcic minerals. In the studied cherts, the Si/(Si+Fe+Al+Ca) ratio ranges from 0.59 to 0.96. This indicates that most silica in cherts originates from biogenic siliceous shells.

The Al–Fe–Mn diagram defined by Yamamoto (1987) has been used for classification of the origin of chert (Fig. 3.6). On this diagram the analyzed chert samples plot close to the Al–Fe line due to extremely low Mn concentrations. All the analyses plot in the field of non-hydrothermal cherts.

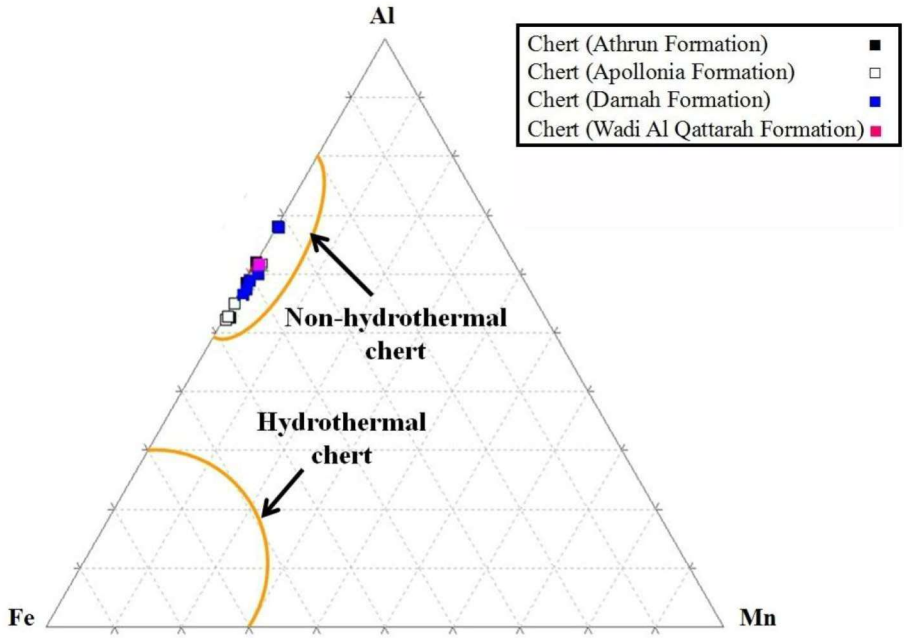

Fig. 3.6: Ternary plots of Al – Fe– Mn for chert samples (fields after Yamamoto, 1987)

Figs (3.7-8) show that all of the samples plot close to Post-Archean Average Shale (PAAS). In the studied samples, a recycled component has not been identified and Zr/Sc changes appear to be due to compositional variations only. High silica addition causes a significant shift toward higher values of the Y/Ni ratio.

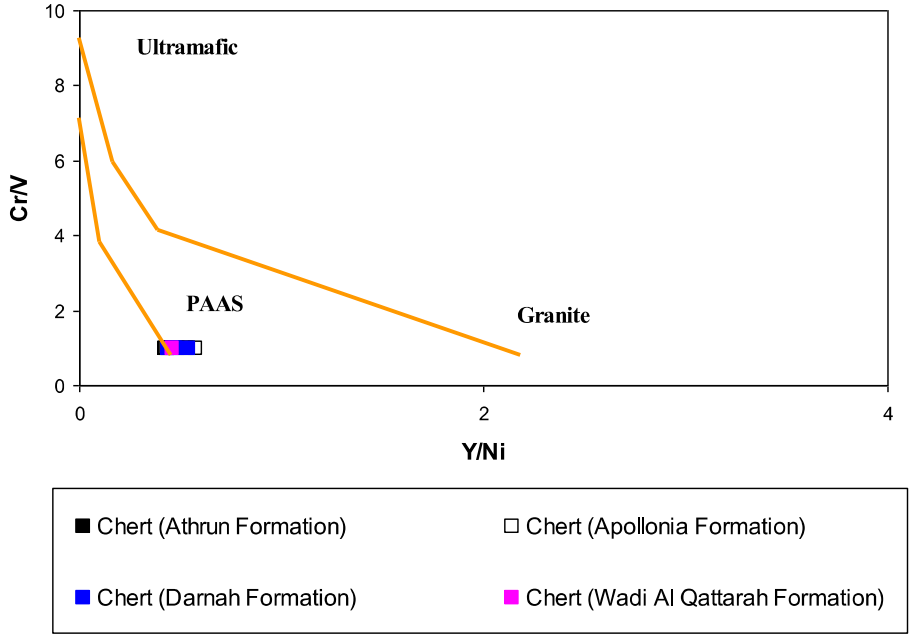

Fig. 3.7: Relationship between Y/Ni and Cr/V in the studied cherts (fields after Hiscott, 1984)

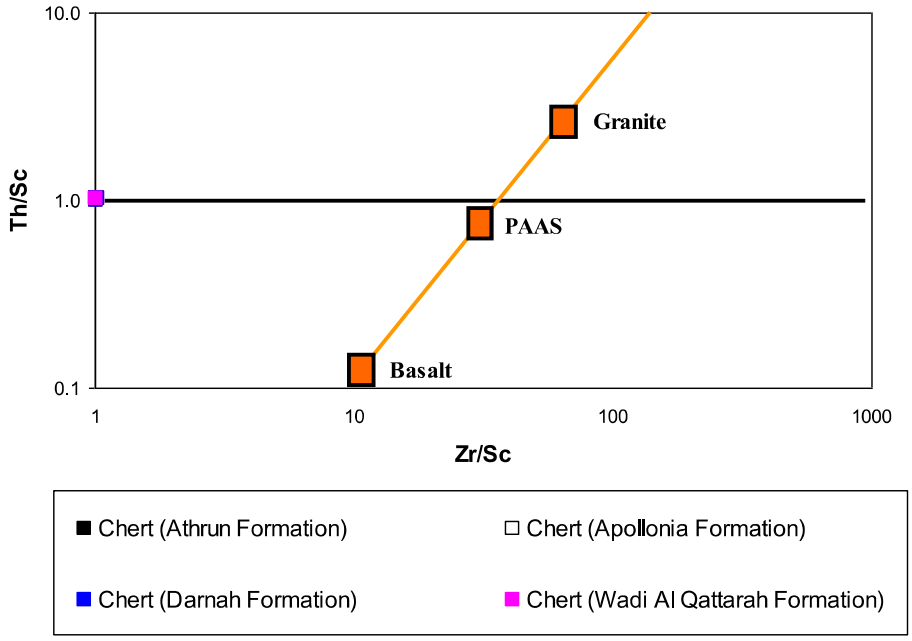

Fig. 3.8: Relationship between Zr/Sc and Th/Sc in the studied cherts (fields after Ran et al., 2015)

Today, most of the silicon influx into the oceans is thought to come from continental weathering because modern seawater Ge/Si is low (~0.72) (Mortlock and Froelich, 1987). In contrast, significant enrichment of Ge in hydrothermal fluids results in 1 order of magnitude higher Ge/Si than that of seawater (~11) (Mortlock *et al.,* 1993). In the studied cherts, the Ge/Si ratio ranges from 0.41 to 0.65 μmol/mol, which is close to the Ge/Si ratio of modern seawater and biogenic silica. The relationships between $\delta^{30}Si$ and the Al_2O_3, TiO_2 and K_2O contents were applied to identify the main silica source and the origin mechanism of ancient cherts (van den Boorn *et al.,* 2007, Ramseyer *et al.,* 2013). Three possible quartz components or Si-bearing precursors can be easily identified in Figs (3.9-11). One silica end-member represents hydrothermal fluids with low Al_2O_3, TiO_2 and K_2O contents, a high Ge/Si ratio and a negative $\delta^{30}Si$ value. Another end-member represents continental detritus and/or volcanic precursors with high Al_2O_3, TiO_2 and K_2O contents, a moderate Ge/Si ratio and a near zero $\delta^{30}Si$ value. The last end-member is diagenetic quartz that is derived from seawater with low Al_2O_3, TiO_2 and K_2O contents, a low Ge/Si ratio and a typically positive $\delta^{30}Si$ value. The studied cherts fall in the field of seawater precipitation (*see* Figs. 3.10-11).

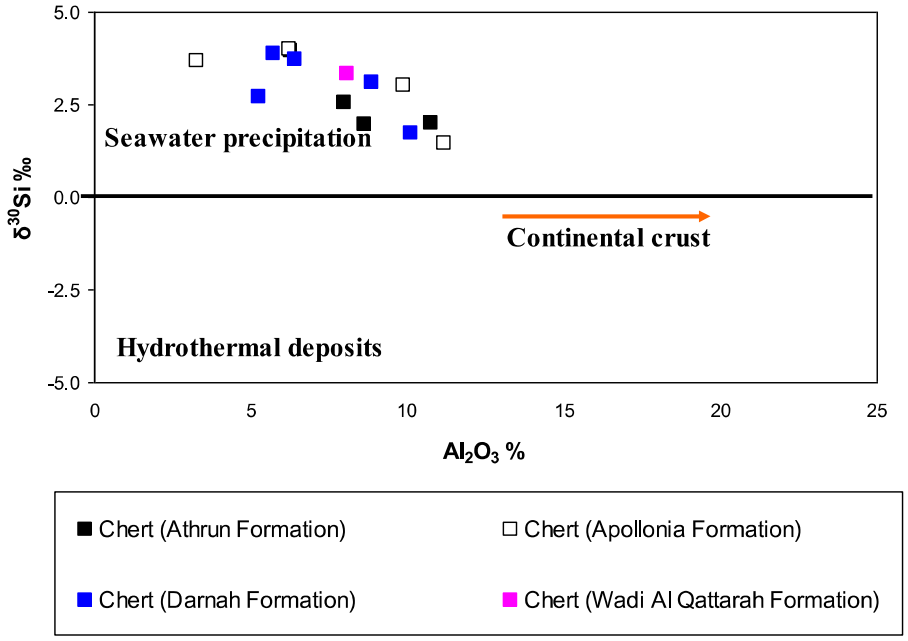

Fig. 3.9: Relationship between Al_2O_3 and $\delta^{30}Si$ in the studied cherts (fields after van den Boorn et al., 2007)

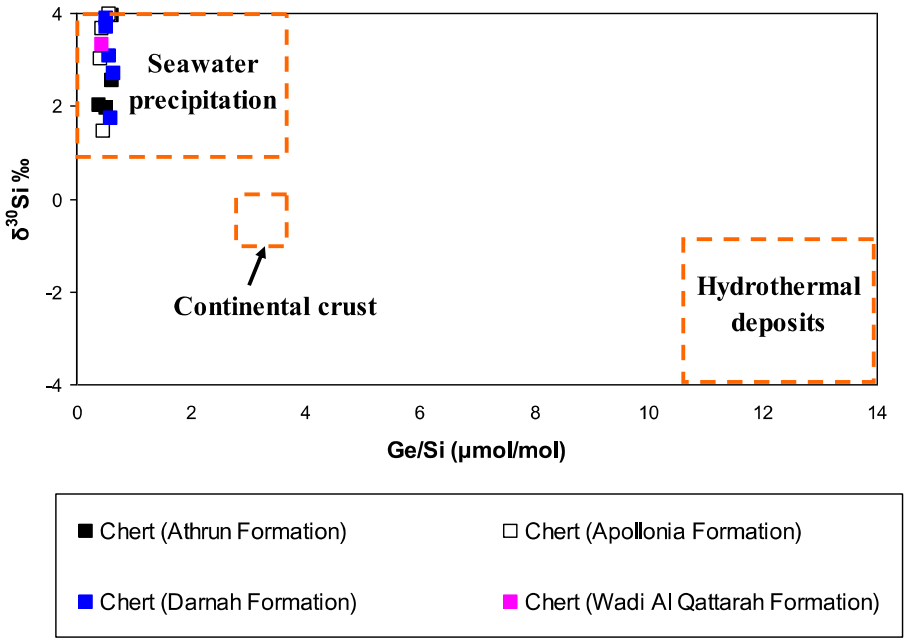

Fig. 3.10: Relationship between Ge/Si and δ^{30}Si in the studied cherts (fields after Wen et la., 2016)

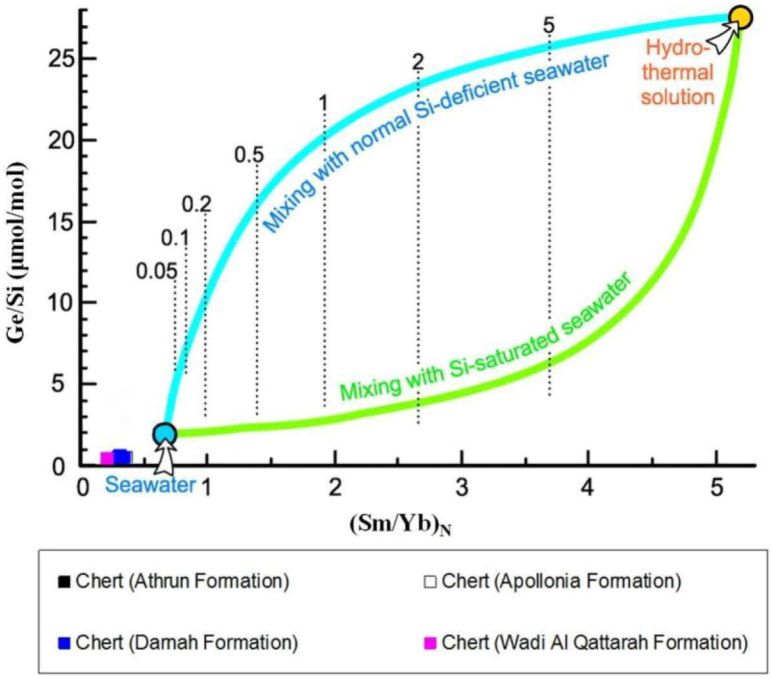

Fig. 3.11: Relationship between $(Sm/Yb)_N$ and Ge/Si in the studied cherts (fields after Grenne and Slack, 2003)

Detrital materials potentially affected the REE + Y patterns of carbonates and cherts due to the high REE contents in silicate minerals. The Al, Sc, and Zr contents and the relationship between these elements and REE are commonly applied to monitor continental silicate detritus contamination (Nothdurft *et al.,* 2004; Ling *et al.,* 2013). According to Wen *et al.,* (2016) a criterion (REE > 20ppm) is applied to define the significant detrital contamination. In the studied samples, the concentration of REE ranges from 4.3 to 13.39. Furthermore, the correlation between Al_2O_3 and REE also suggests that the seawater materials are the main source of REE (Fig. 3.12). The studied samples display low values of ΔCe (0.03-0.11) and high values of Y/Ho ratio (48 to 339.73). According to Murray *et al.,* (1991) open-ocean seawater displays very low ΔCe values (0.2-0.3), continental margin sediments (0.8-1); increasing terrigenous influences increase ΔCe values. The Y/Ho ratios (>45) were examined for modern seawater and were interpreted to reflect preferential scavenging of REE by particulate matter in the seawater column (Nozaki *et al.,* 1997).

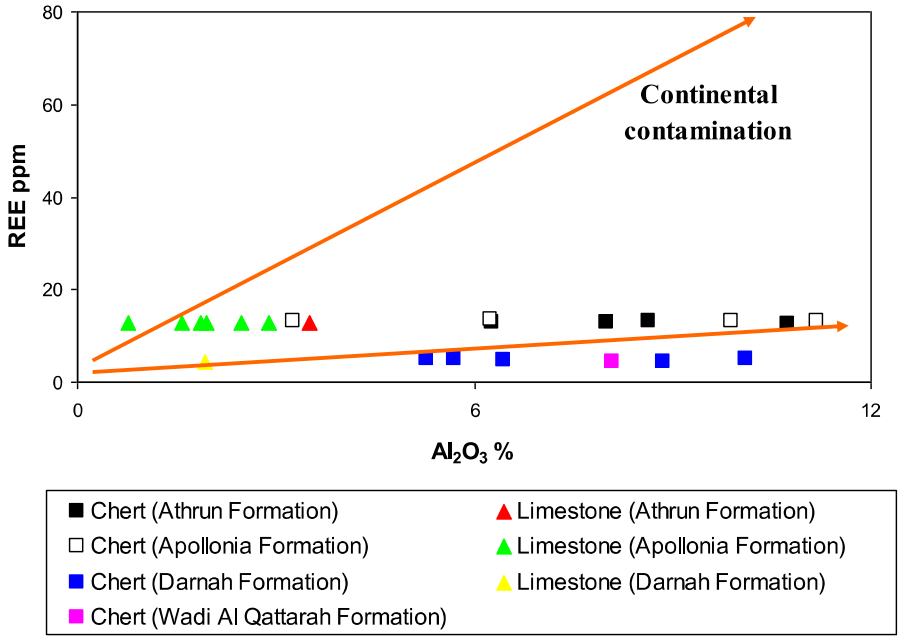

Fig. 3.12: Relationship between Al_2O_3 and REE in the studied samples (fields after Wen et al., 2016)

Shields and Stille (2001) proposed that diagenesis could cause REE patterns to become progressively Ce-enriched, Eu-depleted and $(Dy/Sm)_N$ depleted, although REE in carbonates and cherts are not easily altered after deposition (Webb *et al.,* 2009). However, a weak correlation

between ΔCe and $(Dy/Sm)_N$ ratios has been observed in studied samples (Fig. 3.13), indicating that the REE + Y patterns and Ce anomalies of the studied cherts and limestones have not shifted during the diagenetic processes.

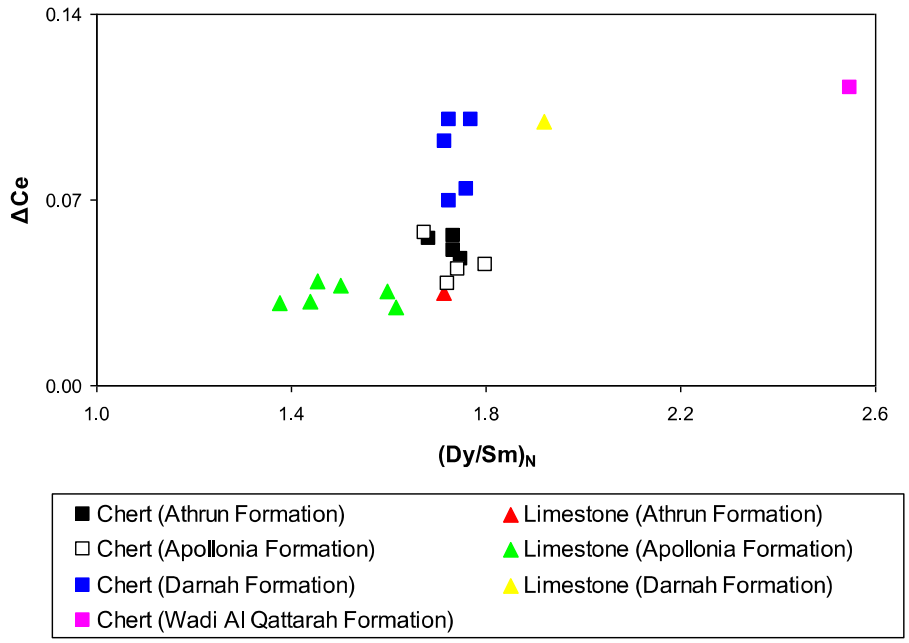

Fig. 3.13: Relationship between $(Dy/Sm)_N$ and ΔCe in the studied samples

According to Bau and Alexander (2009) the chondritic Zr/Hf ratio of 38, indicating that it only fractionates in highly evolved felsic magmas. However, in aqueous systems, Zr–Hf fractionation is more the rule than the exception, as evidence by non-chondritic Zr/Hf ratios in modern seawater (Zr/Hf:56-207; Bau and Alexander, 2009). Modern seawater shows Hf/Ta ratios between 1.3 and 2.5 (Bau and Alexander, 2009); these are lower than the Hf/Ta ratio of the average upper continental crust and that of chondrites. The Zr/Ta ratio of modern seawater ranges from 115 to 688 (Bau and Alexander, 2009). The studied cherts display ratios of seawater almost similar to Hf/Ta (1.32-2.43), Zr/Ta (117.14-357.96), and Zr/Hf (56.55-161.23) (Fig. 3.14). The Th/U ratio in epiclastic sedimentary rocks is not very variable and falls close to the Th/U ratio of average upper continental crust (3.9; Condie, 1993). The studied cherts have mostly high Th/U ratios of 5-14.22 (Fig. 3.15).

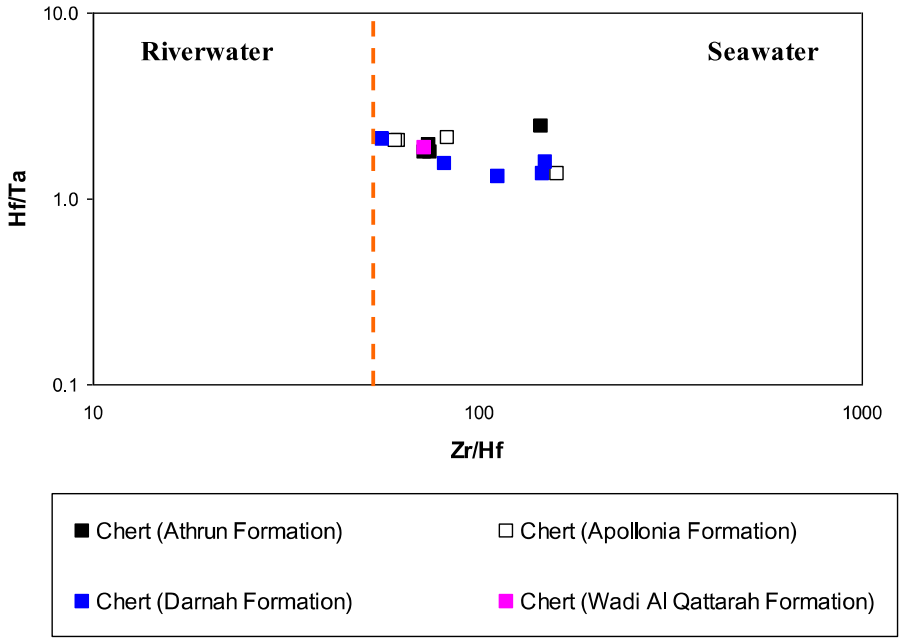

Fig. 3.14: Relationship between Zr/Hf and Hf/Ta in the studied chert samples (fields after Bau and Alexander, 2009)

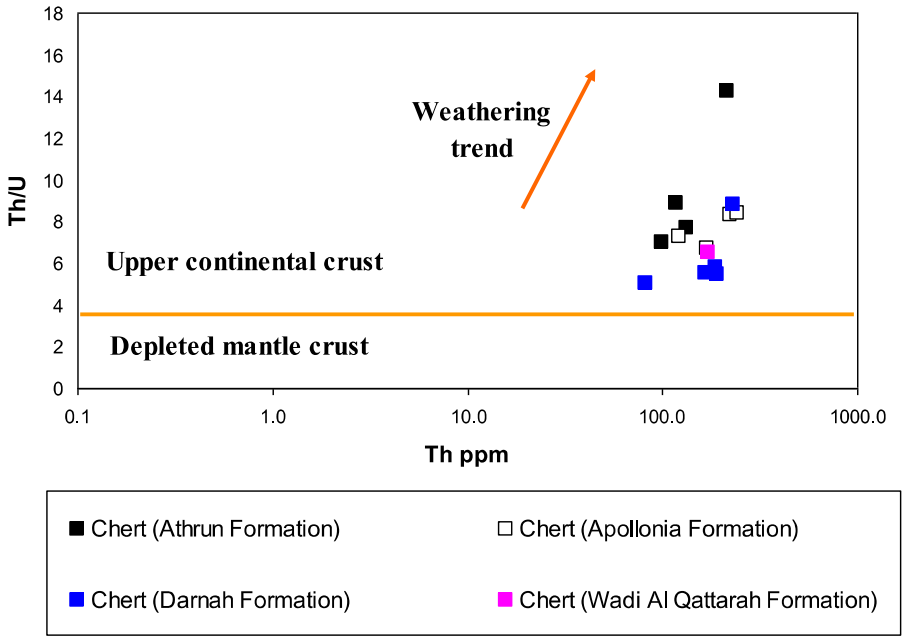

Fig. 3.15: Relationship between Th and Th/U in the studied chert samples (fields after Bau and Alexander, 2009)

The studied cherts have rather low Nb/U values (1.67-10.64) due to high Nb depletion (*see* Fig. 3.1). Fig (3.16) shows that there is no correlation between $(La/Sm)_N$ and Nb/U. It also implies that low Nb/U in the cherts is not attributed to continental contamination.

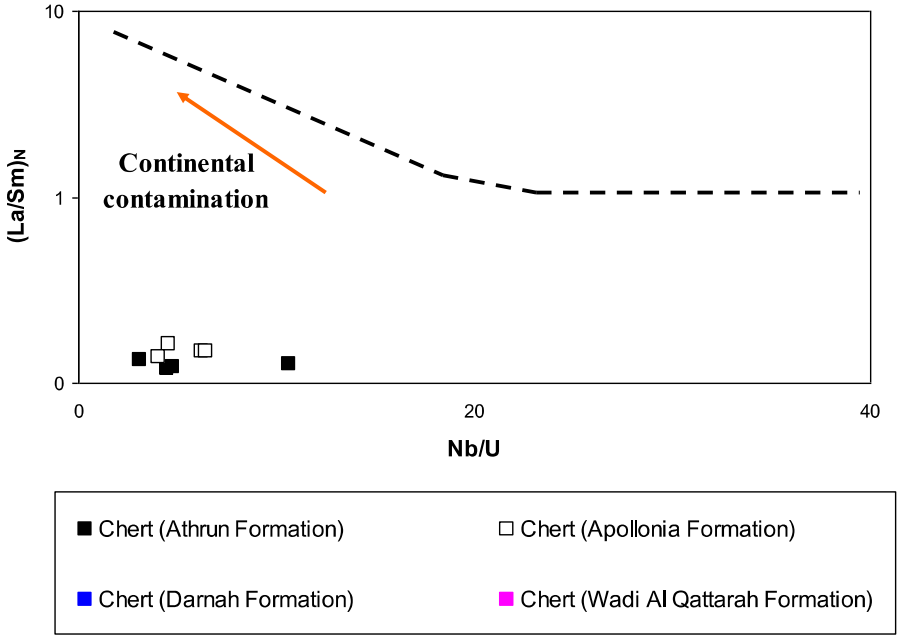

Fig. 3.16: Relationship between Nb/U and $(La/Sm)_N$ in the studied chert samples (fields after Green et al., 2000)

Moreover, the ratios calculated from Ni, Co and V have been used in assessing the origin, depositional environment and in some cases thermal maturity of organic matter (Udo *et al.,* 1992; Akinlua *et al.,* 2010). Enhanced concentration of V over Ni is an indication of marine organic matter input while the reverse is indicative of terrestrial organic matter input (Akinlua *et al.,* 2016). In other word, high V/Ni value indicates values less than 1.9 indicate terrestrial organic matter, V/Ni values from 1.9 to 3 indicate organic matter of mixed marine and terrestrial source input, while V/Ni ratio higher than 3 indicates marine organic matter. The studied chert samples have V/Ni ratio ranging from 3.10 to 3.59, suggesting marine organic matter input. Cross plot constructed from the values of Co/Ni and V/Ni (Fig. 3.17) also indicates that the cherts have marine origin.

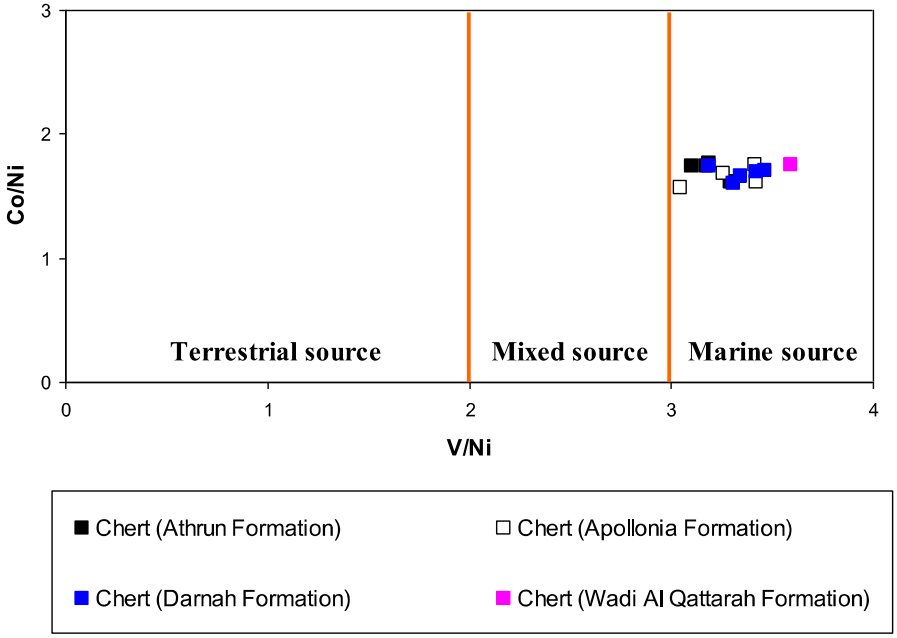

Fig. 3.17: Relationship between V/Ni and Co/Ni in the studied chert samples (fields after Galarraga et al., 2008)

3.8. Depositional environments and paleooxygenation conditions

The REE concentrations in the studied formations are less than typical marine carbonate value (~28 ppm, by Bellanca, 1997). PAAS-normalized REE patterns of the studied samples are shown in Fig (3.18). The studied formations shows more or less flat REE pattern with negative Ce- and Eu anomalies. The PAAS-normalized REE patterns indicate that Athrun and Apollonia formations of deep marine environments, while Darnah and Wadi Al Qattarah formations of shallow marine environments.

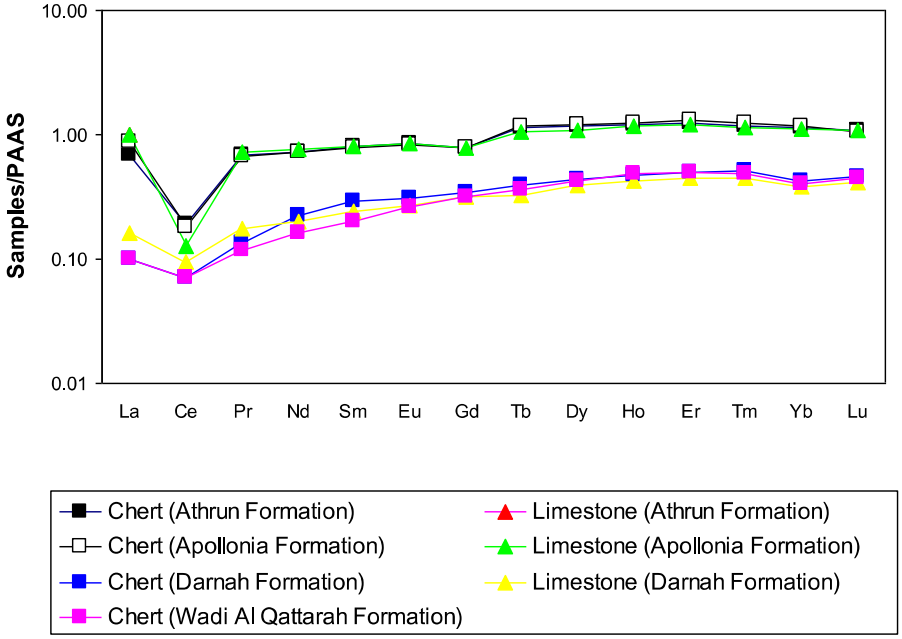

Fig. 3.18: PAAS-normalized REE diagram for the studied formations

Depositional environment has a significant effect on the concentrations of V, Cr, Ni, Co, Th and U in sedimentary rocks (Lewan, 1984). The V/Cr, Ni/Co and U/Th ratios are widely used to indicate redox conditions during sedimentation and diagenesis (e.g., Nagarajan *et al.,* 2007; Shaltami *et al.,* 2016). The studied formations display low values of V/Cr (< 2), Ni/Co (< 5) and U/Th (< 1.25) ratios, which is an indication of deposition under oxic conditions. This interpretation is further supported by the plots of Ni vs. V and Ni/Co vs. V/Cr (Figs. 3.19-20).

Fairly low Al-normalized concentrations of redox-sensitive trace metals (Ni/Al, Co/Al, V/Al and Cr/Al) and the presence of foraminifera in the studied formations confirm that the studied sediments was accumulated in an oxygenated water column.

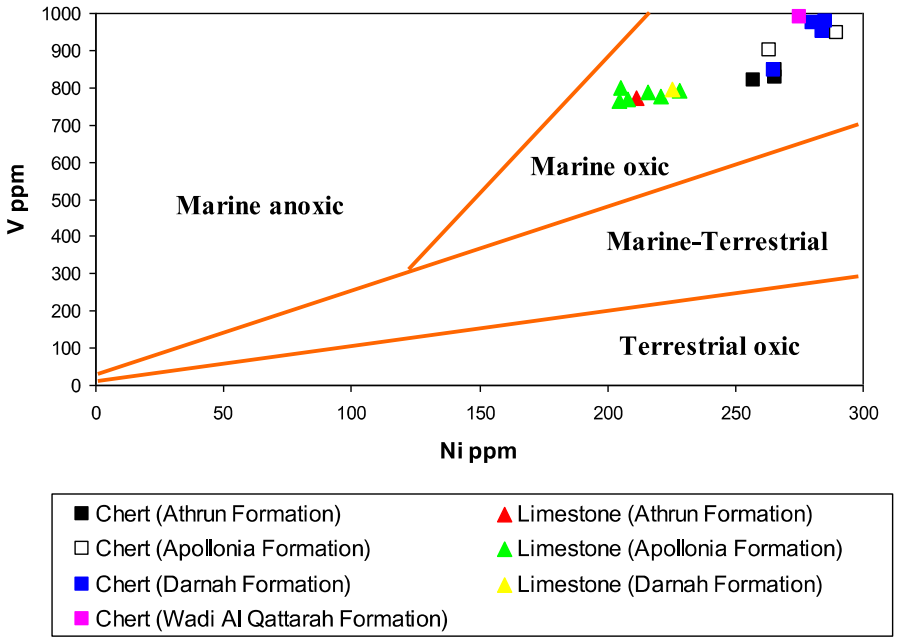

Fig. 3.19: Relationship between Ni and V in the studied samples (fields after Akinlua et al., 2016)

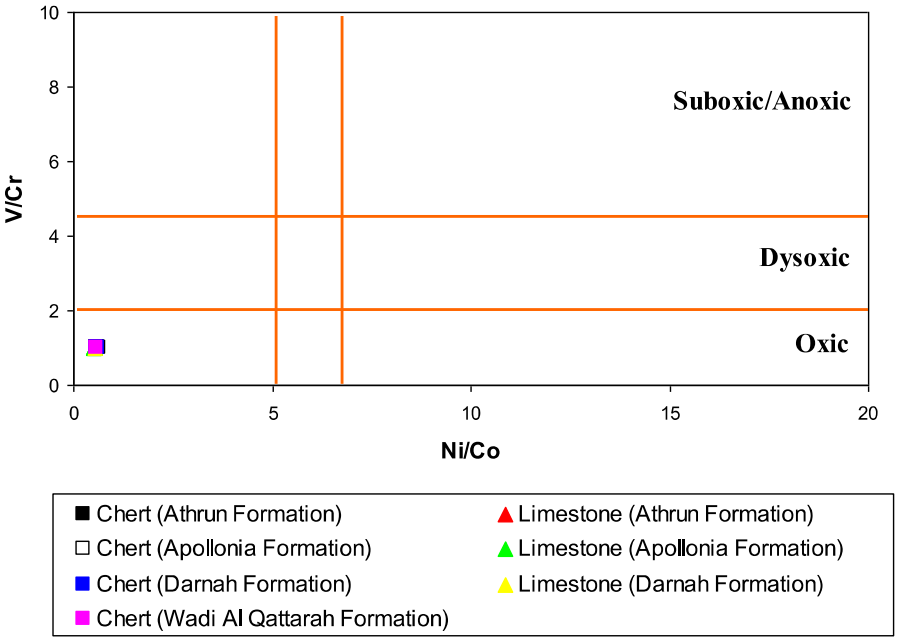

Fig. 3.20: Relationship between Ni/Co and V/Cr in the studied samples (fields after Jones and Manning, 1994)

3.9. Paleoclimate conditions

Climate has extreme effect on mineralogy and geochemistry of sediments (Yan *et al.,* 2010). Weathering is related to climate. Intense weathering (especially chemical) is associated with warm and humid climate whereas minimal weathering is associated with cold and arid climate (Nesbitt *et al.,* 1996). In present study, the plots on the binary SiO_2 versus (Al_2O_3 + K_2O + Na_2O) diagram of Suttner and Dutta (1986) shows that the analyzed sediments were deposited during semi-humid climatic conditions (Fig. 3.21).

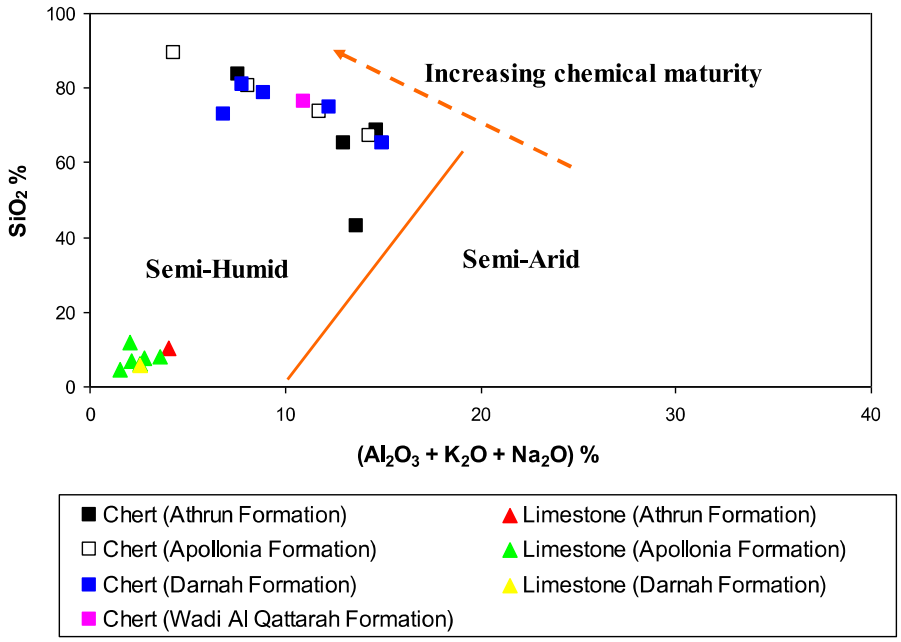

Fig. 3.21: Relationship between SiO_2 and (Al_2O_3 + K_2O + Na_2O) in the studied samples (fields after Suttner and Dutta, 1986)

3.10. Weathering in the source area

A variety of geological issues, including the regulation of long-term climate, the release of nutrients into the biosphere and the control of primary sediment yield derived from rock decomposition, control the system of material recycling upon the Earth's surface due to the prime mechanism of weathering processes (Ohta and Arai, 2007). Identification of mechanism of weathering processes, degree of weathering or various chemical weathering indices are very useful tools in characterizing and determining the extent of weathering. In the A–CN–K diagram (Fig. 3.22) the studied samples plot above the feldspar join line, indicating high to moderate chemical weathering of the source.

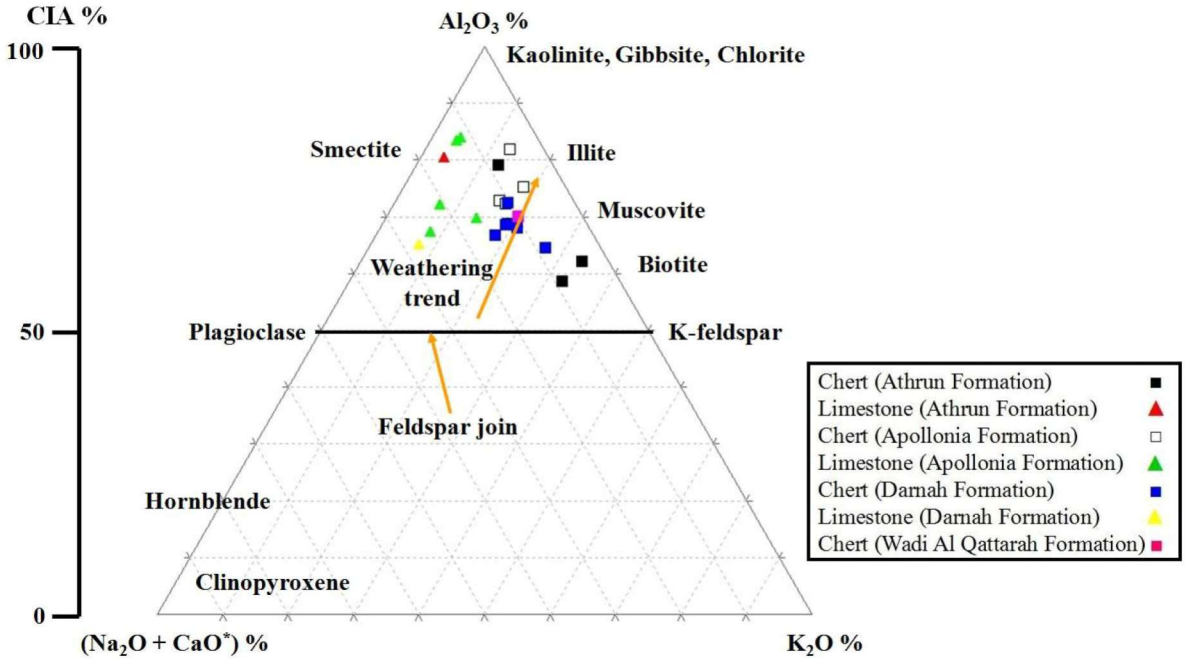

Fig. 3.22: A-CN-K ternary weathering diagram of the studied samples (fields after Nesbitt and Young, 1982)

3.11. Tectonic setting

Major elements distribution in sedimentary rocks is significantly controlled by the tectonic settings of their provenances (e.g., Bhatia, 1983; McLennan and Taylor, 1991; Bakkiaraj *et al.,* 2010; Shaltami *et al.,* 2016). The tectonic diagrams discriminate between Oceanic island Arc (A), continental island Arc (B), active continental margin (C) and passive margin (D). The analyzed samples plot in the fields of D and C (Figs. 3.23-25).

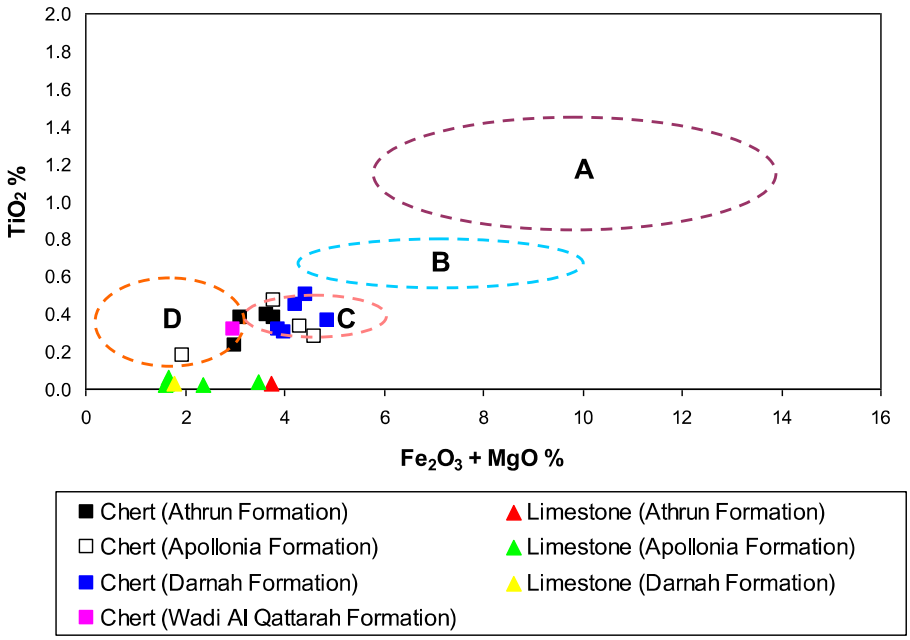

Fig. 3.23: Relationship between (Fe_2O_3 + MgO) and TiO_2 in the studied samples (fields after Bhatia, 1983)

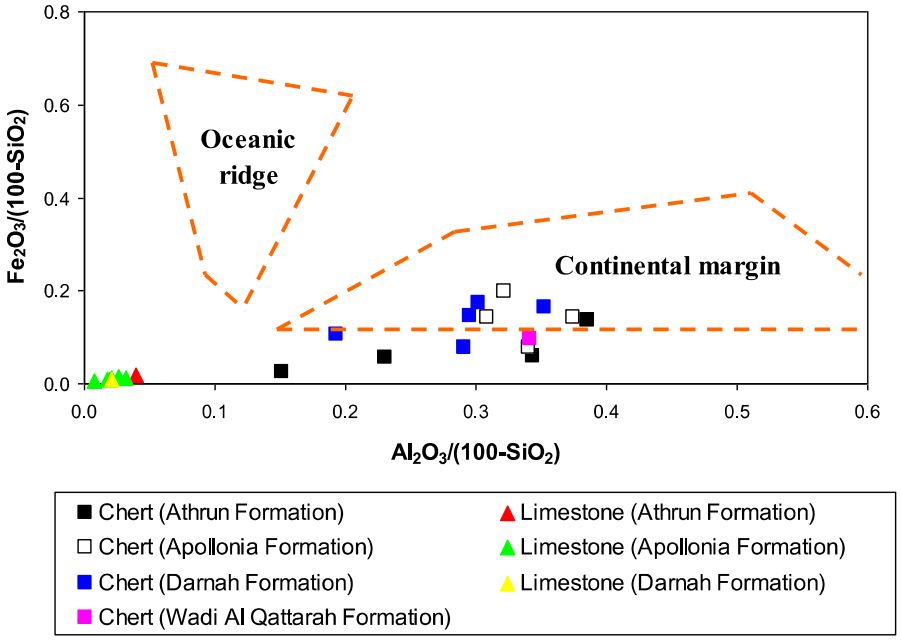

Fig. 3.24: Relationship between $Al_2O_3/(100\text{-}SiO_2)$ and $Fe_2O_3/(100\text{-}SiO_2)$ in the studied samples (fields after He et al., 2011)

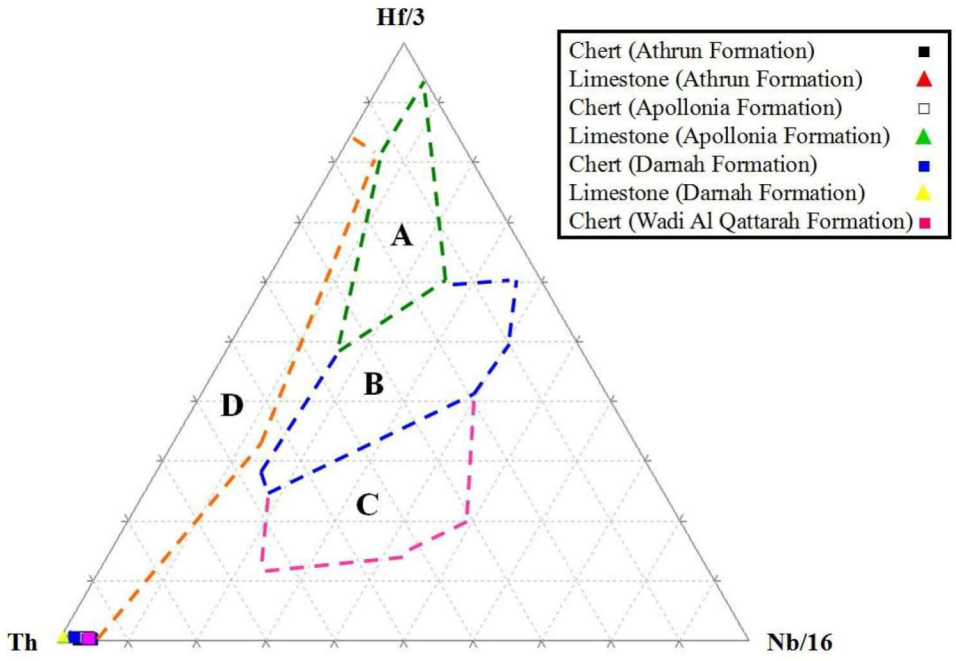

Fig. 3.25: Ternary plots of Hf/3 – Th – Nb/16 for the studied samples (fields after Wood, 1980)

CHAPTER IV
4-CONCLUSIONS

The main objective of the present work is to describe the petrography and geochemistry of the chert nodules and bands at Al Jabal Al Akhdar, NE, Libya, with especial emphases on the origin, depositional environment, tectonic setting, paleoclimate and paleooxygenation condition.

Cherts occur in Al Jabal Al Akhdar at four formations, these are: Al Athrun Formation (Upper Cretaceous), Apollonia Formation (Lower-Middle Eocene), Darnah Formation (Middle-Upper Eocene) and Wadi Qattarah Formation (Upper Miocene).

The microscopic examination indicates that the main siliceous materials in Al Athrun Formation are radiolarian shells, while sponge spicules and inorganic silica (microcrystalline quartz) are the detected siliceous materials in Apollonia and Darnah formations, which are strongly supporting the biogenic origin of these cherts. The only observed siliceous material in Wadi Al Qattarah Formation is microcrystalline quartz.

Geochemically, in the studied cherts, the Al/Si vs. TOC plot indicates that grains carry more TOC than mud. The studied cherts can be rated as having a fair hydrocarbon potential (0.53 to 0.75%).

The ternary plot of Al–Fe–Mn shows that the chert samples fall in the field of non-hydrothermal cherts. The Si/(Si+Fe+Al+Ca), Ge/Si, Hf/Ta, Zr/Ta and Zr/Hf ratios range from 0.59 to 0.96, 0.41 to 0.65μmol/mol, 1.32 to 2.43, 117.14 to 357.96 and 56.55 to 161.23, respectively, which indicate that most silica in cherts originates from biogenic siliceous shells. This interpretation is further supported by the plots of $\delta^{30}Si$ vs. Al_2O_3, Ge/Si vs. $\delta^{30}Si$, $(Sm/Yb)_N$ vs. Ge/Si, Al_2O_3 vs. REE, Zr/Hf vs. Hf/Ta, Nb/U vs. $(La/Sm)_N$ and V/Ni vs. Co/Ni.

The PAAS-normalized REE patterns indicate that Athrun and Apollonia formations of deep marine environments, while Darnah and Wadi Al Qattarah formations of shallow marine environments.

The studied formations display low values of V/Cr (< 2), Ni/Co (< 5) and U/Th (< 1.25) ratios, which is an indication of deposition under oxic conditions. This interpretation is further supported by the plots of Ni vs. V and Ni/Co vs. V/Cr.

The discrimination diagram (SiO_2 vs. (Al_2O_3 + K_2O + Na_2O)) shows that the analyzed sediments were deposited during semi-humid climatic conditions.

In the A–CN–K diagram the samples plot above the feldspar join line, indicating high to moderate chemical weathering of the source. The K_2O/Al_2O_3 ratio ranges 0.05 to 0.3, indicating that clay minerals have a major role in the distribution of aluminum in the chert samples. The presence of clay minerals in the studied cherts is also supported by positive correlation between Al_2O_3 and K_2O + Na_2O.

The tectonic diagrams show that the samples fall in the fields of active continental margin and passive margin.

References

Albarede, F., Telouk, P., Blichert-Toft, J., Boyet, M., Agranier, A. and Nelson, B. (2004): Precise and accurate isotopic measurements using multiple-collector ICPMS. Geochim. Cosmochim. Acta; 68: 2725-2744.

Akinlua, A., Adekola, S.A., Swakamisa, O., Fadipe, O.A. and Akinyemi, S.A. (2010): Trace metals characterisation of Cretaceous Orange Basin hydrocarbon source rocks. App. Geochem.; 25: 1587-1595.

Akinlua, A., Olise, F.S., Akomolafe, A.O. and McCrindle, R.I. (2016): Rare earth element geochemistry of petroleum source rocks from northwestern Niger Delta. Marine and Petroleum Geology; 77: 409-417.

Amrouni, K.S., Pope, M.C., El-Hawat, A.S., Amer, A.; Elbileikia, E.A., El-Bargathi, H.S., Obeidi, A.A., Shaltami, O.R., Mustafa, K.A.M., Al-Alwani, A.M.A., El-Jahmi, M.S.A, El-Ekhfifi, S.S.A. and Wehner, M.P. (2016): Silicification in the Cyrenaican Miocene carbonate-evaporite sequence, NE Libya: Origin, occurrence, facies, and sea level relationship. Gulf Coast Association of Geological Societies Transactions; 66: 29-38.

A. S. El Hawat and M. A. Shelmani,(1993), "Short Notes and Guide Book on the Geology of Al Jabal Al Akhdar Cyrenaica," NE Libya, 70 p.

Bakkiaraj, D.; Nagendra, R.; Nagarajan, R. and Armstrong-Altrin, J.S. (2010): Geochemistry of sandstones from the Upper Cretaceous Sillakkudi Formation, Cauvery Basin, Southern India: Implication for Provenance. Journal of the Geological Society of India; 76: 453-467.

Barr, F. T. and Hammuda, O. S. (1971) Biostratigraphy and planktonic zonation of the Upper Cretaceous Atrun Limestone and Hilal Shale, Northeastern Libya. Proceedings of the II Planktonic Conference, Roma 1970, p. 27-38. Roma.

Barr, F. T. (1972). Biostratigraphy and planktonic zonation of the Upper Cretaceous Atrun Limestone and Hilal Shale, northeastern Libya. In: Proc. 2nd Int. Conf. Plank. Microfossils. A. Farinacci, Ed. Rome, pp. 27-40.

Barr, F.T.and Berggren W.A. (1980). Lower Tertiary Biostratigraphy and Tectonic of NE Libya. In: M.J.Salem & M.T. Busrewil (Eds.), Geology of Libya Academic press, London, V.I, P

Bau, M. and Alexander, B.W. (2009): Distribution of high field strength elements (Y, Zr, REE, Hf, Ta, Th, U) in adjacent magnetite and chert bands and in reference standards FeR-3 and FeR-4 from the Temagami iron-formation, Canada, and the redox level of the Neoarchean ocean. Precambrian Research; 174: 337-346.

Bellanca, A.; Masetti, D. and Neri, R. (1997): Rare earth elements in limestone/marlstone couplets from the Albian-Cenomanian Cismon section (Venetian region, northern Italy): assessing REE sensitivity to environmental changes. Chemical Geology; 141: 141-152.

Bhatia, M.R. (1983): Plate tectonics and geochemical composition of sandstones. Journal of Geology; 92: 181-193.

Bouchez, J., Gaillardet, J., France-Lanord, C., Maurice, L. and Dutra-Maia, P. (2011): Grain size control of river suspended sediment geochemistry: Clues from Amazon River depth profiles, Geochem. Geophys. Geosyst., 12, Q03008, doi:10.1029/2010GC003380.

Botz, R., Stoffers, P., Faber, E. and Tietze, K. (1988): Isotope geochemistry of carbonate sediments from Lake Kivu (East–Central Africa). Chemical Geology; 69: 299-308.

Brand, U. (1989): Biogeochemistry of Late Paleozoic North American brachiopods and secular variations of sea water composition. Biogeochemistry; 7: 159-193.

Brand, U. and Veizer, J. (1980): Chemical diagenesis of a multicomponent carbonate system, 1. Trace elements. J. Sediment. Petrol., 50: 1219-1236.

Buckley, D.E. and Cranston, R.E. (1991): The use of grain size information in marine geochemistry, In: Principles, Methods and Applications of particle size analysis, Syvitski, J. M. (Ed.), Cambridge Univ. Press, New York. Geol. Survey of Canada Contrib., 12689: 311-331.

Connant, L.C and Goudarzi, G. H.1964, Geological map of the kingdom of Libya U.S. Geol. Survey misc. Geol.Inv. map1-350A, scale 1: 2,000,000

Chave, K.E. (1962): Processes of carbonate sedimentation. Narragansett Marine Lab. Occ. Publ.; 1: 77-85.

Condie, K.C. (1993): Chemical composition and evolution of the upper continental crust: contrasting results from surface samples and shales. Chemical Geology; 104: 1-37.

Cox, R.; Low, D.R. and Cullers, R.L. (1995): The influence of sediment recycling and basement composition on evolution of mudrock chemistry in the southwestern United States. Geochim. Cosmochim. Acta; 59: 2919-2940.

El Amawy, M. A., Muftah, A. M., Abdel Wahed, M. and Nassar,(2011). A. Wrench structural deformation in Ras Al Hilal-Al Athrun area, NE Libya: A new contribution in Northern Al Jabal Al Akhdar belt. Arab. J. of Geosci., , 4: 1067-1085.

El Arnauti, A., A. Lawrece, S . R., Mansouri, A. L., Celal Sengor,A. M, Soulsb, A., Hassan, H., (2008), structural styles in NE Libya. Geology of east Libya, ,vol.4,pp.153-178.

El Hawat, A. S. and Shelmani, M. A., (1993): Short notes and guidebook on the geology of Al Jabal alAkhdar, Cyrenaica, NE Libya. Imprinted Limited Malta, 70p.

El Hawat A. S. and Abdulsamad E. O., (2004). A field guide to the geology and archaeology of Cyrenaica. In: 32nd International Geological Congress, Special Public.

El Hawat, A. S., Jorry, S., Caline, B., Davaud, E., Masse, P. (2008): The Ypresian-Early Lutetian Facies, Sequences, and Unconformities of Cyrenaica: Their Correlation and Implications in North Africa. Geology of East Libya, Vol. 1: 85-120

El Khoudary, R. H. (1980). Planktonic foraminifera from the Middle Eocene of the Norhtern escarpment of Al Jabal al Akdar, NE Libya. In: M.J. Salem and M.T. Busrewil (Eds.), The Geology of Libya. Academic Press, London, I : 193-204.

El-Mehaghag, A. A., and Muftah, A. M, (1996): Calcareous nannofossils and foraminiferal biostratigraphy of Al Hilal Formation, North-East Libya. In: The 3th International conference on the Geology of the Arab World, Cairo University, 501-520.

EL Mehaghg A. A and EL Mehdawi A. D (2006) : A review of the calcareous nannofossils biostratigraphy of the Al Athrun and apollonian Formation, cyrerenaica, NE Libya . J. Nannoplankton Res; 28 (2) . 89-93

El Mehaghg A. A, Muftah, A.M Daw, S.I (2008): Biostratigraphy evaluation of Tukrah Formation in Cyrenica, NE Libya. The Geology of East Libya. M-J Salem, A. El- Arnaut. A.E.Saleh (eds), Gutenbery press . ltd, Malta 3, 163-170

Erik Flugel., (2010). Microfacies of Carbonate Rocks Analysis, Interpretation and Application Second Edition.,Springer, 984p.

El-Shafeiy, M., Birgel, D., El-Kammar, A., El-Barkooky, A., Wagreich, M., Omar M. and Peckmann, J. (2014): Palaeoecological and post-depositional changes recorded in Campanian-Maastrichtian black shales, Abu Tartur plateau, Egypt. Cretaceous Research; 50: 38-51.

Elwerfli, A.O., Muftah, A. M. and EL Hawat, A.S. (2000). A Gidbook on the geology of Al Jabal Al Akhdar.Crenica.NE Libya. Gutenberg press, malta; 71:6.

Elwerfali, H. Stow, D.(2008), Facies analysis of early tertiary carbonates in NE Libya, geology of east Libya ,vol. 1, pp. 121-152

Fan, H., Zhu, X., Wen, H., Yan, B., Li, J. and Feng, L. (2014): Oxygenation of Ediacaran Ocean recorded by iron isotopes. Geochimica et Cosmochimica Acta; 140: 80-94.

Folk, R.L. (1980): Petrology of Sedimentary Rocks. Hemphill, Austin, TX, 79.

Galarraga, F., Llamas, J.F., Martinez, A., Martinez, M., Marquez, G. and Reategui, K. (2008): V/Ni ratio as a parameter in palaeoenvironmental characterization of nonmature medium-crude oils from several Latin American basins. J. Petrol. Sci. Eng.; 61: 9-14.

Gary, N. (2009) Sedimentology and stratigraphy. 2nd ed. A John Wiley and Sons, Ltd., Publication.

Green, M.G., Sylvester, P.J. and Buick, R. (2000): Growth and recycling of early Archean continental crust: geochemical evidence from the Coonterunah and Warrawoona Groups, Pilbara Craton, Australia. Tectonophysics; 322: 69-88.

Gregory, J.W., (1911). Contributions to the geology of Cyrenaica Quart. J.Geol.Sco, London, p. 36.

Grenne, T. and Slack, J.F. (2003): Paleozoic and Mesozoic silica-rich seawater: Evidence from hematitic chert (jasper) deposits. Geology; 31:319-322.

Goudarzi, G H. (1970). Geology and Mineral resources of Libya – A reconnaissance. U. S. Geol. Surv., Prof. Pap., 660, 104 p.

Hay, W. W. (1968). Coccoliths and other calcareous nannofossils in marine sediments in Cyrenaica. In Geology and archaeoiogp of Northern Cyrenaica, Libya, p. 149-157. ‘Tripoli.

Helmdach, F .and El khoudary, R(1980), Ostracoda and plnkktonic Formainifera from the late Eocene of Al Jabal Al Khdar, Northeastern of Libya,In:The geology of Libya (eds m.J.salem and M.T(Busrewil). Acadmic press. london, I255-269.

He, J., Zhou, Y. and Li, H. (2011): Study on geochemical characteristics and depositional environment of Pengcuolin chert, Southern Tibet. Journal of Geography and Geology; 3(1): 178- 188.

Hesse, R. (1988): Origin of chert: diagenesis of biogenic siliceous sediments. Geoscience Canada; 15: 171-192.

Hiscott, R.N. (1984): Ophiolitic source rocks for Taconic-age flysch: Trace-element evidence. Geological Society of America Bulletin; 95: 1261-1276.

Jones, B. and Manning, D.C. (1994): Comparison of geochemical indices used for the interpretation of paleo-redox conditions in Ancient mudstones: Chemical Geology; 111(1-4): 111-129.

Kato, Y. and Nakamura, K. (2003): Origin and global tectonic significance of Early Archean cherts from the Marble Bar greenstone belt, Pilbara Craton, Western Australia. Precambrian Research; 125(3-4): 191-243.

Kempl, J., Vroon, P.Z., Zinngrebe, E. and van Westrenen, W. (2013): Si isotope fractionation between Si-poormetal and silicate melt at pressure–temperature conditions relevant to metal segregation in small planetary bodies. Earth Planet. Sci. Lett.; 368: 61-68.

Klen, L., 1974. Geological Map of Libya; 1:250 000. Sheet NI 34-14, Bengahzi, and explanatory booklet. Indust. Resear. Cent., Tripoli, 56 pp.

Lewan, M.D. (1984): Factors controlling the proportionality of vanadium to nickel in crude oils. Geochimica et Cosmochimica Acta; 48: 2231-2238.

Ling, H.F., Chen, X., Li, D., Wang, D., Shields-Zhou, G.A. and Zhu, M. (2013): Cerium anomaly variations in Ediacaran-earliest Cambrian carbonates from the Yangtze Gorges area, South China: Implications for oxygenation of coeval shallow seawater. Precambrian Research; 225: 110-127.

McLennan, S.M. and Taylor, S.R. (1991): Sedimentary rocks and crustal evolution: tectonic setting and secular trends. Journal of Geology; 99: 1-21.

Molenaar, N. and Jong, A.F.M (1987): Authigenic quartz and albite in Devonian limestone: Origin and significance. Sedimentology; 34: 623-640.

Mortlock, R.A. and Froelich, P.N. (1987): Continental weathering of germanium: In the global river discharge, Geochim. Cosmochim. Acta; 51(8): 2075-2082.

Mortlock, R.A., Froelich, P.N., Feely, R.A., Massoth, G.J., Butterfield, D.A. and Lupton, J.E. (1993): Silica and germanium in Pacific Ocean hydrothermal vents and plumes, Earth Planet. Sci. Lett., 119(3): 365-378.

Morton, A.C. (1985): A new approach to provenance studies: Electron microprobe analysis of detrital garnets from Middle Jurassic sandstones of the northern North Sea. Sedimentology; 32: 553-566.

Muftah, A. M., El Faitouri, M. E. and El Khufafai, S. (2015): Utilization of the observed geological features in differentiating the exposed rock units in Al Jabal al Akhdar, Libya. Omn, Pubblishe.171-178

Murray, R.W. (1994): Chemical criteria to identify the depositional environment of chert: general principles and applications. Sedimentary Geology; 90: 213-232.

Murray, R.W., Buchholtz ten Brink, M.R., Gerlach, D.C., Ruth III, G.P. and Jones, D.L. (1991): Rare earth, major, and trace elements in chert from the Franciscan Complex and Monterey Group, California: assessing REE sources to fine-grained marine sediments. Geochim. Cosmochim. Acta; 55: 1875-1895.

Murray, R.W., Buchholtz ten Brink, M.R., Gerlac, D.C., Russ III, G.P. and Jones, D.L. (1992): Interoceanic variation in the rare earth, major, and trace element depositional chemistry of chert: perspectives gained from the DSDP and ODP record. Geochimica et Cosmochimica Acta; 56: 1897-1913.

Nagarajan, R.; Madhavaraju, J.; Nagendra, R.; Armstrong-Altrin, J.S. and Moutte, J. (2007): Geochemistry of Neoproterozoic shales of the Rabanpalli Formation, Bhima Basin, Northern Karnataka, southern India: implications for provenance and paleoredox conditions. Revista Mexicana de Ciencias Geológicas; 24 (2): 150-160.

Nesbitt, H.W. and Young, G.M. (1982): Early Proterozoic climates of sandstone mudstone suites using SiO_2 content and K_2O/Na_2O ratio. Nature; 299: 715-717.

Nesbitt, H.W., Young, G.M., McLennan, S.M. and Keays, R.R. (1996): Effects of chemical weathering and sorting on the petrogenesis of siliciclastic sediments, with implications for provenance studies. J. Geol.; 104: 525-542.

Nothdurft, L.D., Webb, G.E. and Kamber, B.S. (2004): Rare earth element geochemistry of Late Devonian reefal carbonates, canning basin, Western Australia: Confirmation of a seawater REE proxy in ancient limestones. Geochimica et Cosmochimica Acta; 68: 263-283.

Nozaki, Y., Zhang, J. and Amakawa, H. (1997): The fractionation between Y and Ho in the marine environment. Earth and Planetary Science Letters; 148: 329-340.

Ohta, T. and Arai, H. (2007): Statistical empirical index of chemical weathering in igneous rocks: A new tool for evaluating the degree of weathering. Chemical Geology; 240: 280-297.

Peters, K.E. and Cassa, M.R. (1994): Applied source rock geochemistry. In: Magoon, L.B., Dow, W.G. (Eds.): The petroleum system from source to trap, AAPG, Mem.; 60: 93-117.

Pietersz C. R., (1968). Proposed nomenclature for rock units in Northern Cyrenaica. In Geology and Archaeology of Northern Cyrenaica, Libya. Soc. Libya, Tripoli.

Qi, L., Hu, J. and DC, G. (2000): Determination of trace elements in granites by inductively coupled plasma mass spectrometry. Talanta; 51: 507-513.

Raczek, I., Stoll, B., Hofmann, A.W. and Peter Jochum, K. (2001): High-precision trace element data for the USGS reference materials BCR-1, BCR-2, BHVO-1, BHVO-2, AGV-1, AGV-2, DTS-1, DTS-2, GSP-1 and GSP-2 by ID-TIMS and MIC-SSMS. Geostand Newslett; 25: 77-86.

Ramseyer, K., Amthor, J.E., Matter, A., Pettke, T., Wille, M. and Fallick, A.E. (2013): Primary silica precipitate at the Precambrian/Cambrian boundary in the South Oman Salt Basin, Sultanate of Oman. Marine and Petroleum Geology; 39: 187-197.

Ran, B., Liu, S., Jansa, L., Sun, W., Yang, D., Ye, Y., Wang, S., Luo, C., Zhang, X. and Zhang, C. (2015): Origin of the Upper Ordovician–Lower Silurian cherts of the Yangtze block, South China, and their palaeogeographic significance. Journal of Asian Earth Sciences; 108: 1-17.

Rangin, C., Steinberg, M. and Bonnot-Courtois, C. (1981): Geochemistry of the Mesozoic bedded cherts of Central Baja California (Vizcaino-Cedros-San Benito): implications for paleogeographic reconstruction of an old oceanic basin. Earth and Planetary Science Letters; 54: 313-322..

Rohlich P., (1974). Geological map of Libya; 1:250,000, Sheet Al Bayda NI34-15. Explanatory Booklet. Industrial Research Centre, Tripoli, 70 pp.

Rohlich, P. (1978) Tectonic development of Al Jabal Al Akhdar 2nd symp on the Geology of Libya; Rund., Al Fateh University, Tripoli, Libya. 2,pp. 410-412.

Rohlich P., (1980). Tectonic Development of Al Jabal Al Akhdar. In: The Geology of Libya (eds Salem M.J., Buserwil M.T.). Academic Press, London, III, P. 923-931.

Shields, G. and Stille, P. (2001): Diagenetic constraints on the use of cerium anomalies as palaeoseawater redox proxies: an isotopic and REE study of Cambrian phosphorites. Chemical Geology; 175: 29-48.

Shaltami, O.R., Fares, F.F. and Bustany, I. (2016): Geochemistry of Mamuniyat Formation, Idri area, SW Libya. 11th International Conference and Meeting on Geology, Institute of Geosciences, University of Campinas, Brazil, Proceeding Book; pp. 88-102.

Starkies., keejan,J B., Mansori,.A.L.,Yanilmaz, E.,El-Arnauti, A.(2007).stratigraphic nomenclature of northeast Libya. Wellstrat services limited, uk, 169p.

Sugisaki, R., Yamamoto, K. and Adachi, M. (1982): Triassic bedded cherts in central Japan are not pelagic. Nature; 298: 644-647.

Sun, S., Schefub E., Mulitza, S., Chiessi, C.M., Sawakuchi, A.O., Zabel, M. Baker, P.A., Hefter, J. and Mollenhauer, G. (2016): Origin and processing of terrestrial organic carbon in the Amazon system: lignin phenols in river, shelf and fan sediments. Biogeosciences Discuss., doi:10.5194/bg-2016-468.

Suttner, L.J. and Dutta, P.K. (1986): Alluvial sandstone composition and paleoclimate. Framework mineralogy. Journal of Sedimentary Petrology; 56: 326-345.

Taylor, S.R. and McLennan, S.M. (1985): The Continental Crust: its composition and evolution. Blackwell Scientific Publishers, Oxford.

Udayanapillai, A.V. and Ganesa Moorthi, P. (2014): Mineralogy and geochemistry of the red and black sediments of the Tuticorin district, Tamilnadu, India. Journal of Geological society of Srilanka; 15: 47-56.

Udo, O.T., Ekwere, S. and Abrakasa, S. (1992): Some trace metal in selected Niger Delta crude oils: application in oil-oil correlation studies. J. Min. Geol.; 28: 289-291.

van den Boorn, S.H.J.M., van Bergen, M.J., Nijman, W. and Vroon, P.Z. (2007): Dual role of seawater and hydrothermal fluids in Early Archean chert formation: Evidence from silicon isotopes. Geology; 10: 939-942.

van den Boorn, S.H.J.M., Vroon, P.Z. and van Bergen, M. (2009): Sulphur-induced offsets in MC-ICP-MS silicon-isotopes measurements. J. Anal. At. Spectrom.; 24: 1111-1114.

Veizer, J. (1978): Secular variations in the composition of sedimentary carbonate rocks, 11. Fe, Mn, Ca, Mg, Si and minor constituents. Precambrian Research; 6: 381-413.

Veizer, J., Lemieux, J., Jones, B., Gibling, M.R. and Savelle, J. (1977): Sodium: Paleosalinity indicator in ancient carbonate rocks. Geology (Boulder); 5: 177-179.

Webb, G.E., Nothdurft, L.D., Kamber, B.S., Kloprogge, J.T. and Zhao, J. (2009): Rare earth element geochemistry of scleractinian coral skeleton during meteoric diagenesis: a sequence through neomorphism of aragonite to calcite. Sedimentology; 56: 1433-1463.

Wen, H., Fan, H., Tian, S., Wang, Q. and Hu, R. (2016): The formation conditions of the early Ediacaran cherts, South China. Chemical Geology; 430: 45-69.

White, A.F. (1977a): Sodium and potassium coprecipitation in aragonite. Geochimica et Cosmochimica Acta; 41: 613-625.

Wilkinson, B.H. and Given, R.K. (1986): Secular variation in abiotic marine carbonates: constraints on Phanerozoic atmospheric carbon dioxide contents and oceanic Mg/Ca ratios. J. Geol., 94: 321-334.

Wood, D.A. (1980): The application of the Th-Hf-Ta diagram to problems of tectonomagmatic classification and establishing the nature of crustal contamination of Basaltic Lava of the British Tertiary Volcanic Province. Earth and Planetary Science; Letters: 50: 11-30.

Yamamoto, K. (1987): Geochemical characteristics and depositional environments of cherts and associated rocks in the Franciscan and Shimanto Terranes. Sedimentary Geology; 52(1-2): 65-108.

Yan, D., Chen, D., Wang, Q. and Wang, J. (2010): Large-scale climatic fluctuations in the latest Ordovician on the Yangtze block, South China. Geology; 38: 599-602.

Yu, B., Dong, H., Widom, E., Chen, J. and Lin, C. (2009): Geochemistry of basal Cambrian black shales and cherts from the Northern Tarim Basin, Northwest China: Implications for depositional setting and tectonic history. Journal of Asian Earth Sciences; 34(3): 418-436.

Zambardi, T. and Poitrasson, F. (2011): Precise determination of silicon isotopes in silicate rock reference materials by MC-ICP-MS. Geostand. Geoanal. Res.; 35: 89-99.

Zert, B. (1974). Geologic map of Libya, 1: 250,000 Dernah sheet NI 34-16, explanatory booklet. Inds. Resear. Cent., Tripoli, 49 pp.

الخلاصة

هذا العمل يناقش الخصائص الصخرية الجيوكيميائية لرواسب الصوان في منطقة الجبل الأخضر شمال شرق ليبيا، توجد رواسب الصوان في تكوينات الاثرون، ابولونيا، درنة ووادي قطارة. من الناحية الصخربة المواد السيليكاتية في رواسل الصوان هي اصداف الردولاريا في تكوين لاثرون والاسفنجيات والكوارتز الدقيق التبلر في تكوينات ابولونيا ودرنة، بينما الكوارتز الدقيق التبلر هو المادة السيليكاتية الوحيدة في تكوين وادي قطارة. من الناحية الجيوكيميائية فان رواسب الصوان أصلها من الكائنات الحية ويدل على ذلك نسب الجرمانيم/السيلكون والهفنيم/التنتانم والزوركونيم/الهفنيم كما ان رواسب الصوان المدروسة هي من نوع الغير حراري مائي. تدل نسب العناصر الثقيلة على ان رواسب الصوان ترسبت في ظروف مؤكسدة. كما ان الوضع التكتوني لهذه الرواسب هو قاري.